EXERGOECONOMIC ANALYSIS OF A DIRECT STEAM SOLAR POWER PLANT IN YEMEN

2023
MASTER THESIS
MECHANICAL ENGINEERING

ABDLRAHMAN AL-TAMIMI

Thesis Advisor
Assist. Prof. Dr. Abdulrazzak Ahmed Saleh AKROOT

EXERGOECONOMIC ANALYSIS OF A DIRECT STEAM SOLAR POWER PLANT IN YEMEN

Abdulrahman AL-TAMIMI

Thesis Advisor
Assist. Prof. Dr. Abdulrazzak Ahmed Saleh AKROOT

T.C.
Karabük University
Institute of Graduate Programs
Department of Mechanical Engineering
Prepared as
Master Thesis

KARABÜK
June 2023

I certify, that in my opinion, the thesis submitted by Abdulrahman AL-TAMIMI titled " EXERGOECONOMIC ANALYSIS OF A DIRECT STEAM SOLAR POWER PLANT IN YEMEN" is fully adequate in scope and in quality as a thesis for the degree of Master of Science.

APPROVAL

Assist. Prof. Dr. Abdulrazzak Ahmed Saleh AKROOT .....
Thesis Advisor, Department of Mechanical Engineering

This thesis is accepted by the examining committee with a unanimous vote in the Department of Mechanical Engineering as a Master of Science thesis. 22/06/2023

Examining Committee Members (Institutions)	Signature
Chairman: Assoc. Prof. Dr. Daver ALİ (KBU)	.....
Member: Assoc. Prof. Dr. Ümit AĞBULUT (DOU)	.....
Member: Assist. Prof. Dr. Abdulrazzak A. S. AKROOT (KBU)	.....

The degree of Master of Science by the thesis submitted is approved by the Administrative Board of the Institute of Graduate Programs, Karabük University.

Prof. Dr. Müslüm KUZU .....
Director of the Institute of Graduate Programs

This thesis contains information that I have gathered and presented in a manner that is consistent with academic regulations and ethical principles, and I affirm that I have appropriately cited any and all sources that are not my own work.

Abdulrahman AL-TAMIMI

ABSTRACT

M. Sc. Thesis

AN EXERGOECONOMIC ANALYSIS OF A DIRECT STEAM SOLAR POWER PLANT IN YEMEN

Abdulrahman AL-TAMIMI

Karabük University
Institute of Graduate Programs
The Department of Mechanical Engineering

Thesis Advisor:
Assist. Prof. Dr. Abdulrazzak Ahmed Saleh AKROOT
June 2023, 77 pages

Increasing reliance on fossil fuels for electrical power generation has a devastating impact on the environment. The proportion of renewable energy sources must be increased to fulfil energy demand and reduce thermal emissions. Frequently, energy storage is required for dispatchable and reliable power generation from renewable sources. This study evaluates the thermodynamic and exergoeconomic analyses of a novel power plant in Aden, Yemen, for the entire system and its subsystems, which include parabolic trough solar collectors, thermal energy storage, and a Rankine cycle. The parametric studies are conducted to determine the effects of severalimportant factors on the performance of the novel system by applying the engineering equation solver software; these analyses are simulated. The impacts of the amount of solar radiation, the boiler's pinch point, turbine isentropic efficiency,

the extraction ratio from the turbines, pressure at the inlet of each turbine, and condenser temperature on system performance and cost were investigated. The results showed the system's overall energy and exergy efficiencies were 29.88% and 31.5%, respectively. The total power produced by the system was 39 MW, and the average system's cost rate was 24.84 $/h.

The findings also present that the exergy destruction in the system directly affects the investment cost. The system's total exergy destruction cost was 906.52 $/h, and the exergoeconomic factor for the design was 78.2%.

Keywords **:** Solar, Thermal Energy Storage, Yemen, Exergoeconomic, Exergoeconomic Factor.

Science Code : 91436

ÖZET

Yüksek Lisans Tezi

YEMEN'DEKİ DOĞRUDAN BUHARLI GÜNEŞ ENERJİSİ SANTRALİNİN EKSERGOEKONOMİK ANALİZİ

Abdulrahman AL-TAMIMI

Karabük Üniversitesi
Lisansüstü Programlar Enstitüsü
Makine Mühendisliği Bölümü

Tez Danışmanı:
Dr. Öğretim Üyesi Abdulrazzak Ahmed Saleh AKROOT
Haziran 2023, 77 sayfa

Elektrik enerjisi üretimi için fosil yakıtlara olan bağımlılığın artması, çevre üzerinde yıkıcı bir etkiye sahiptir. Enerji talebini karşılamak ve termal emisyonları azaltmak için yenilenebilir enerji kaynaklarının oranı artırılmalıdır. Sıklıkla, yenilenebilir kaynaklardan sevk edilebilir ve güvenilir enerji üretimi için enerji depolaması gerekir. Bu çalışma, Yemen, Aden'deki yeni bir enerji santralinin tüm sistem ve parabolik oluk güneş kollektörleri, termal enerji depolama ve bir Rankine çevrimi içeren alt sistemleri için termodinamik ve eksergoekonomik analizlerini değerlendirmektedir. Mühendislik denklem çözücü yazılımı uygulanarak yeni sistemin performansı üzerindeki birkaç önemli faktörün etkilerini belirlemek için parametrik çalışmalar yapılır; bu analizler simüle edilmiştir. Güneş ışınımı miktarının, kazanın sıkışma noktasının, türbin izantropik veriminin, türbinlerden ekstraksiyon oranının, her bir türbin girişindeki basıncın ve kondenser sıcaklığının sistem performansı ve maliyeti üzerindeki etkisi incelenmiştir. Sonuçlar, sistemin

genel enerji ve ekserji verimliliklerinin sırasıyla %29.88 ve %31.5 olduğunu gösterdi. Sistemin ürettiği toplam güç 39 MW, ortalama sistem maliyeti ise 24,84 $/h olarak gerçekleşti. Bulgular ayrıca sistemdeki ekserji yıkımının yatırım maliyetini doğrudan etkilediğini ortaya koymuştur. Sistemin toplam ekserji yok etme maliyeti 906.52 $/h ve tasarım için eksergoekonomik faktör %78.2 idi.

Anahtar Kelimeler : Güneş, Termal enerji depolama, Yemen, Eksergoekonomik, Eksergoekonomik faktör.

Bilim Kodu : 91436

ACKNOWLEDGEMENT

O Allah, benefit me with what you have taught me and teach me what will benefit me, and increase my knowledge. Praise be to God, with Whose grace good deeds are accomplished, and thanks to Whom blessings perpetuate. And prayers and peace be upon the best of creation, our Prophet Muhammad and his good and pure family and companions, I dedicate this humble effort to those who have led me from the beginning to the shore of success, to those who raised me when I was young, encouraged me, raised my status, supported me in their prayers and supplications, and did not hold anything back for the sake of my comfort and success, and taught me that the world is a struggle and its weapon is science and knowledge to my sun and moon, my dear father and dear mother, those who, no matter what I do and write, do not fulfill their right, you are the light of my path.

To those whom I had in this world, my Wife, Safia MUKRED and my Son Tameem ALTAMIMI and my brother Mohammad ALTAMIMI, who supported me and accompanied me throughout the study period and gave everything he could to complete this work.

To my Teacher and Teachers, Assist. Prof. Dr. Abdulrazzak Ahmed Saleh AKROOT, who was credited with teaching me, providing advice and guidance, and expressing his opinion throughout the study period, and who has been the best reference for me. I also thank the head of the Department of Mechanical Engineering, Prof. Dr. Kamel Arslan, and his staff.

To everyone who supported me and extended a helping hand, I also dedicate this achievement to my dear country, YEMEN, and my beloved city, TAIZ, steadfast in its people, and to the country that hosted me throughout my study period, Turkey.

CONTENTS

Sayfa

Sayfa

LIST OF FIGURES

Sayfa

Sayfa

LIST OF TABLES

Sayfa

SYMBOLS AND ABBREVITIONS INDEX

SYMBOL

A_a	Solar collector area (m^2)
c_p	Specific heat (kJ/kg. K)
$\dot{C}_{D,k}$	Cost of exergy destruction ($/h)
$\dot{C}_{el}$	Unit cost of electricity produced ($/kWh)
$\dot{C}$	Cost rate ($/h)
DNI	Direct normal irradiation (kWh/ m^2. day)
$\dot{E}$	Energy (kW)
$\dot{E}x$	Exergy (kW)
$\dot{E}x_D$	Rate of exergy destruction (kW)
f_k	Thermoeconomic factor (%)
F_R	Collector heat gain factor
h	Specific enthalpy (kJ/kg)
i	Interest rate
k	Conductivity heat transfer (W/m. K)
l	Insulation thickness (m)
$\dot{m}$	Mass flow rate (kg/s)
n	Predicted life of the system's (years)
P	Pressure (bar)
$\dot{Q}$	Heat rate (kW)
$\dot{Q}_{\text{Solar}}$	Solar Energy input (kW)
r_k	Relative cost variance (%)
s	Specific entropy (kJ/kg. K)
S	Amount of absorbed solar radiation (W/m^2)
T	Temperature (°C)
U_L	Heat loss coefficient of the collector (W/m^2. K)

ν	Specific volume (m^3/kg)
$\dot{W}$	Power (kW)
$\dot{W}$	Work done by the control volume per unit time (kW)
Z	Initial investment cost ($)
ε	Exergy efficiency (%)
Δt	Charging time (s)
φ	Total operating and maintenance cost factor
ψ	Specific exergy (kJ/kg)

ABBREVITIONS

b	Boiler
c	Condenser
CRF	Capital Recovery Factor
CSP	Concentrated solar power
FPCs	Flat Plate Collectors
GT	Gas turbine
GTIT	Gas turbine inlet temperature
HE	Heat exchanger
HESS	Hydrogen Energy Storage System
HRB	Heat recovery boiler
HRSG	Heat recovery steam generation
in	Inlet
ISCC	Integrated solar combined cycle
LHS	Latent heat storage
NGCC	Natural gas combined cycle
ORC	Organic Rankine cycle
ORT	Organic Rankine turbine
out	Outlet
P	Pump
PV	Solar photovoltaics
RC	Cycle
SHS	Sensible heat storage
ST	Steam Turbine

TCES	Thermochemical storage
TES	Thermal energy storage
th	Thermal
PEC	Purchase equipment cost

CHAPTER ONE

INTRODUCTION

1.1. GENERAL

Renewable energy is critical because it is clean and sustainable, and it can help us lessen our dependency on fossil fuels. Fossil fuels significantly contribute to climate change, and renewable energy may help minimize the consequences of climate change. Furthermore, renewable energy is becoming more economical and widely available, making it a feasible choice [1].

Renewable energy comes in numerous forms, including solar, wind, hydropower, geothermal, and biomass. Each renewable energy source has benefits and disadvantages. Solar energy, for example, is plentiful and clean, yet it might be intermittent due to weather conditions. Wind energy is also abundant and environmentally friendly even though it may be loud and unattractive. Hydroelectric energy is a dependable source of electricity, yet it may be harmful to the environment. Geothermal energy is a safe and reliable energy source, but it is not accessible everywhere. Although biomass energy is a sustainable energy source, it may be land-intensive and contribute to air pollution [2,3].

Renewable energy integration into power plants is a challenging problem, but it is critical to the transition to a sustainable energy future. Renewable energy sources such as the sun and wind are intermittent, so they only provide power when these energy sources are available. This may cause issues for power plants, which must provide a consistent stream of energy to fulfil demand [4].

There are numerous approaches to incorporating renewable energy into power plants. The essential method is to employ energy storage technology to store extra power

when generated and then release it back into the plant as required. Renewable energy integration into the power plant is a continuous process. The integration of renewable energy into power plants will become more significant as the cost of renewable energy technology continues to decline and the demand for clean energy develops [5].

Thermal energy storage (TES) systems present viable options to address the incongruity between the availability and utilization of solar energy while providing enhanced system longevity and reliability [6]. Integrating Thermal Energy Storage (TES) systems with eco-innovative storage materials can decrease reliance on non-renewable energy sources, enhance energy efficiency and sustainability, and augment the industry's competitiveness [7].

1.2. SOLAR ENERGY PERSPECTIVE

Solar energy is a renewable energy source that has the potential to satisfy a large amount of the world's energy requirements. Solar photovoltaics (PV), solar thermal, and concentrated solar power (CSP) are all technologies that can capture the sun's energy. The world's solar energy potential is spread differently. Some areas receive far more sunshine than others, but solar energy is a viable source, even in areas with less sunlight [8,9].

In recent years, there has been a reduction in the cost of solar energy, thereby rendering it more economically feasible and comparable to alternative energy sources. Solar power is a renewable and environmentally friendly energy option that does not generate harmful emissions such as greenhouse gases or other contaminants. Given the decreasing cost of solar energy and the increasing demand for sustainable energy sources, it is anticipated to assume a progressively significant position within the worldwide energy portfolio [10].

There are several advantages to using solar energy in industrial applications, including the fact that [11]:

- It is a renewable energy source that will never finish.
- It is becoming more cost-effective.
- It is clean and sustainable since it emits no greenhouse emissions or other pollutants.
- It is a dependable energy source that may create power even during peak demand times.
-

There are several challenges to using solar energy in industrial applications, including the fact that:

- It is an intermittent energy source which does not always provide power.
- It requires a significant initial investment.
- Solar panels need a large quantity of land.
- Solar panels are susceptible to damage from sleet, precipitation, and other atmospheric conditions.

Despite these difficulties, solar energy is a promising renewable energy source that has the potential to satisfy a considerable amount of the world's energy demands [12].

1.3. SOLAR COLLECTOR

Solar collectors are devices that collect solar radiation from the sun and transform it into heat. The appropriate selection of the collector type is a critical determinant that impacts on the efficacy of the solar system. The primary factors to consider when choosing collector types are mounting space, roof design, temperature ranges for application, climate properties, and installation costs [13,14].

There exist various types of collectors in the solar industry that cater to the diverse requirements of users. Solar collectors can be categorized into two distinct groups, namely non-concentrating and concentrating collectors [15], as illustrated in Figure 1.1.

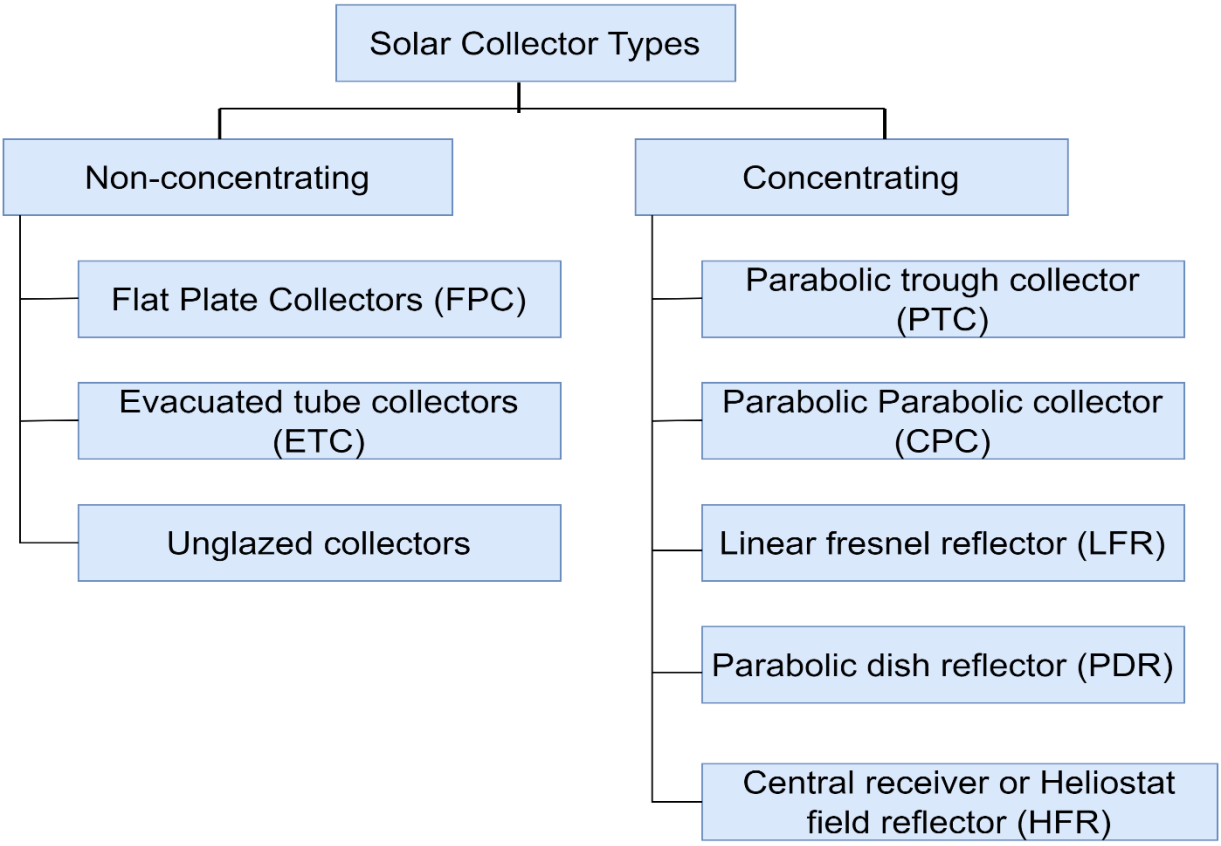

Figure 1. 1. Solar collector types

1.3.1. Non-Concentrating Collectors

Non-concentrating collectors are often preferred in building applications and low-temperature industrial operations. These might involve functions such as room heating, water heating, and other related functions [16].

Flat Plate Collectors (FPCs) are widely utilized for space heating, the production of domestic hot water, and low-temperature manufacturing heat. Figure 1.2 presents a schematic representation of an FPC. The concept behind an FPC is straightforward. Solar radiation is utilized to heat a dark, flat surface called a plate or absorber sheet, which changes the solar radiation energy into heat energy. This heat is then conveyed to the fluid circulating through the attached pipelines [17].

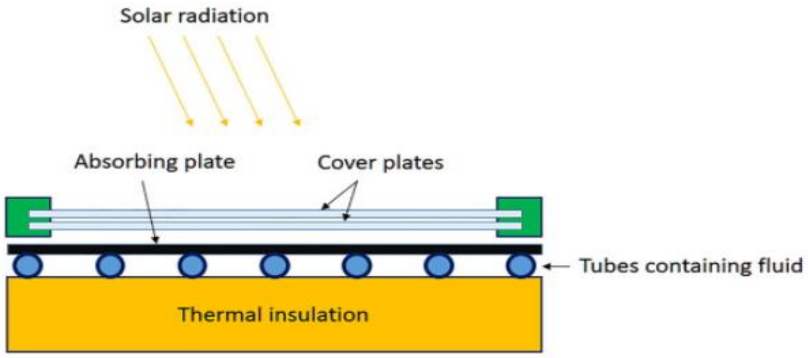

Figure 1. 2. A schematic representation of FPC [17]

1.3.2. Concentrating Collector

Concentrating collectors comprise concentrators and receivers, rendering them suitable for deployment in high-temperature applications such as power generation facilities and manufacturing processes that operate at elevated temperatures [18].
The parabolic trough collector (PTC) is a variant of the concentrating solar thermal collector that employs parabolic mirrors to reflect and focus solar radiation onto a receiver tube. The heat transfer fluid [19] within the receiver tube is subjected to concentrated solar radiation, increasing thermal energy. Subsequently, the high-temperature heat transfer fluid produces steam, which propels a turbine and generates electrical power. Figure 1.3 shows a schematic of a PTC [20].

PTCs are an established technology and have been utilized for over 30 years to produce power. They are a low-cost method of generating power from solar energy that may be employed in a range of regions. A number of the benefits of using PTCs include the following [21]:

- They can be used in a variety of climates.
- They are a cost-effective way to generate electricity from solar energy.
- They are a mature technology with a proven track record.

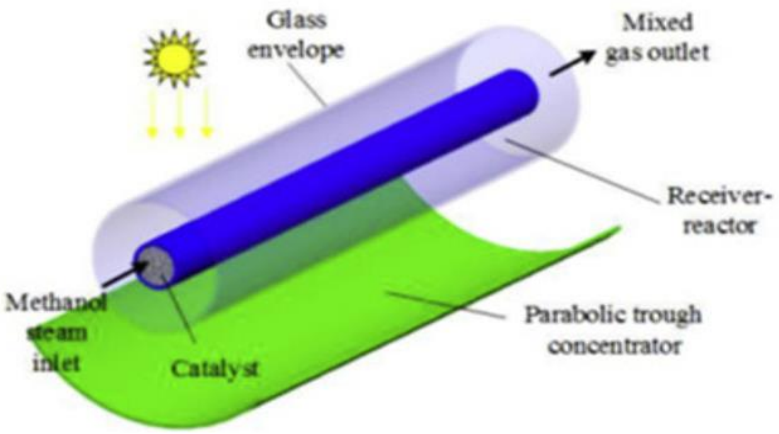

Figure 1. 3. A schematic of PTC [20].

1.4. THERMAL ENERGY STORAGE (TES)

Thermal energy storage (TES) refers to accumulating and retaining heat or cold energy for subsequent utilization. TES has the capability to accumulate energy from diverse sources such as solar, wind, geothermal, and waste heat [22]. The basic flow diagram for a thermal energy storage process is shown in Figure 1.4. When excess hot or cold energy is available, it is used to charge the storage. The storage is discharged when a demand for such power exists, as mentioned in [23]. The storage period in between can vary from a few hours to months.

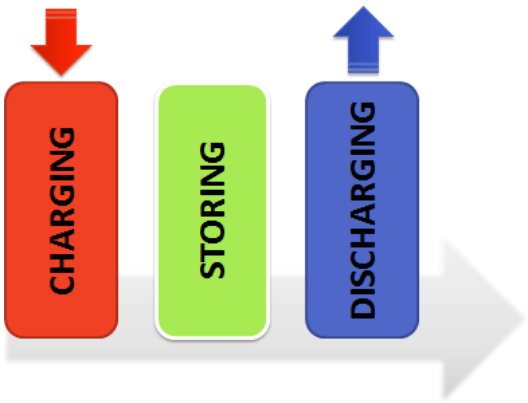

Figure 1. 4. Flow diagram of a thermal energy storage process.

TES is a technology that exhibits great potential to significantly impact the energy landscape in the future. The implementation of TES has the potential to mitigate our dependence on non-renewable energy sources, enhance the dependability of the

power grid, and promote the sustainability of our energy infrastructure. The following are some of the benefits of TES:

- Enhancing grid reliability is a potential outcome.
- The implementation of this approach has the potential to enhance the sustainability of our energy system.
- The implementation of alternative energy sources has the potential to decrease our dependence on non-renewable fossil fuels.

The following are some of the disadvantages of TES:

- It can be costly to install and maintain.
- It can be challenging to indicate the appropriate storage materials.
- TES systems can take time to scale up.

A diverse range of TES technologies exists, each with distinct merits and flaws. Several frequently used TES technologies comprise [24]:

- Sensible heat storage.
- Latent heat storage.
- Thermochemical storage.

1.4.1. Sensible Heat Storage (Shs)

Sensible heat storage (SHS) is a form of thermal energy storage (TES) that retains thermal energy by increasing the temperature of a substance. The thermal energy that has been accumulated can be subsequently discharged through a reduction in the temperature of the substance [25]. SHS is the most used type of TES and is employed in several applications, such as [26]:

- **Solar thermal systems**: SHS is a mechanism used to accumulate and retain heat obtained from solar collectors. This stored heat can be subsequently utilized for the purpose of heating water or indoor spaces.

- **Industrial processes:** SHS is employed to retain thermal energy generated from industrial processes, with the intention of its subsequent utilization.
- **Building heating and cooling:** SHS is a viable option for retaining thermal energy, either in the form of heat or cold, to be subsequently employed in heating or cooling.

The utilization of SHS as a TES technology is considered to be a cost-effective and straightforward approach. Nevertheless, there exist certain constraints associated with it, such as [27,28]:

- The energy density of SHS being comparatively low, thereby necessitating a substantial volume for the storage of a considerable amount of energy.
- The process of heat loss in SHS possibly occurring through three mechanisms, namely conduction, convection, and radiation, which may result in a decrease in the efficacy of the TES system.

SHS is a promising TES technology with many uses despite these drawbacks. SHS is predicted to grow in popularity as the price of TES technology decreases. A number of benefits of SHS include [27]:

- It's cheap and straightforward technology.
- It's coming in several forms and configurations; and
- It's sufficiently versatile to store a wide range of temperatures.

1.4.2. Latent Heat Storage (Lhs)

The change in phase of a substance allows for the storage and release of heat, making latent heat storage a thermal energy storage. Latent heat storage uses the heat absorbed or released during a phase transition, such as melting or solidification, as opposed to sensible heat storage, which depends on raising or lowering the temperature of a material. This method of storing heat is widely used because of its benefits [29].

In the charging stage, a solid or liquid substance undergoes a phase transition to a liquid or a gas state as a result of being heated. The material absorbs the heat energy and stores it as latent heat without considerably raising its temperature. During the discharging phase, when the material experiences the opposite phase transition, the latent heat is released and may be put to use in a variety of ways, including heating and cooling [30].

Compared to more traditional forms of thermal energy storage, latent heat provides a number of benefits, such as [27,31]:

- LHS having a high energy density because it can store a high amount of energy in a small space;
- Rapid heat conduction/dissipation occurring in LHS media; and
- LHS materials having a very long service life since they do not degrade over time.

LHS materials do, however, have a number of drawbacks [27]:

- The materials used to store latent heat tend to be costlier than those used to store thermal energy in more common forms.
- There is a shortage of certain latent heat storage materials.
- Materials used for latent heat storage may need to be handled in a certain way, such as being stored at a consistent temperature; and
- Certain materials for storing latent heat are not extensively accessible.

1.4.3. Thermochemical Storage (Tces)

Thermochemical storage refers to a form of thermal energy storage that entails the retention and discharge of heat using reversible chemical reactions. Thermal energy is stored and released through the absorption or release of energy during chemical reactions. TCES is currently being investigated as a viable solution for thermal energy storage due to its potential to provide efficient and high-capacity storage capabilities [32].

TCES is still in the early stages of development, but it has the potential to be a major breakthrough in energy storage. The technology of TCES has the potential to facilitate the storage of energy derived from renewable sources, including solar and wind power, and also serves as a reliable backup power source during periods of power outages [33].

TCES has the following advantages [32]:

- TCES has a high energy density and can store a large quantity of energy in a small volume.
- TCES can store energy over extended periods of time without deterioration.
- TCES may be very efficient, with conversion efficiencies of up to 90%; and
- TCES is a dependable technology that is not impacted by weather conditions.

TCES, on the other hand, has some disadvantages:

- The cost of materials and components is still high because TCES is a new technology.
- TCES systems are complicated, requiring careful design and operation; and
- TCES is still in its early phases of development, and there is more research that needs to be done.

1.5. AIM OF THE STUDY

The significance of augmenting research endeavors on the utilization of alternative energy sources in Yemen as a means to alleviate acute shortages of electricity is of paramount importance. Yemen is currently facing a critical electricity crisis, with frequent power outages and a significant shortfall in supply. This crisis has had a detrimental impact on the daily lives of Yemeni citizens, affecting essential services such as healthcare, education, and economic activities.

The exploration and utilization of alternative energy sources is crucial in Yemen due to the copious availability of renewable energy resources, such as wind and solar power. Yemen has the potential to generate electricity in a sustainable and environmentally friendly manner by investing in research studies that focus on alternative energy. Renewable energy technologies, such as photovoltaic solar panels and wind turbines, have the potential to be widely implemented throughout the nation to harness its abundant solar irradiance and reliable wind patterns.

Enhancing research efforts in this domain would facilitate Yemen in devising pioneering technologies and solutions customized to its distinct circumstances. Identifying the most appropriate renewable energy systems and optimizing their performance in Yemen's distinct geographical, climatic, and economic circumstances would be beneficial. Furthermore, scholarly investigations can tackle the obstacles associated with assimilating unconventional energy sources into the current power infrastructure and examine feasible energy retention remedies to guarantee a consistent and dependable electricity provider.

Moreover, adopting alternative energy sources can reduce Yemen's dependence on expensive imported fuels, thus easing the economic strain imposed on the country.

This research aims to develop a comprehensive structure for integrating a solar-powered Rankine cycle with thermal energy storage to suit the conditions of Aden, Yemen. The city of Aden, located in Yemen, encounters notable obstacles in electricity production and distribution. The geographical area in question exhibits elevated levels of solar irradiance and possesses the capacity to exploit solar power efficiently. This study aims to enhance the utilization of solar energy and mitigate the acute electricity deficit in Aden, Yemen. The achieved objectives of thermodynamic and exergoeconomic analysis of the combined solar-Rankine cycle with thermal energy storage are summarized as follows:

- The solar resource potential in Aden, Yemen has been analyzed to determine the optimal solar energy collection system configuration.

- The combined solar-Rankine cycle with the thermal energy storage unit has been modelled, taking into account the local environmental conditions.
- The performance of the combined system under varying solar radiation levels and ambient conditions specific to Aden, Yemen have been simulated.
- The system design and operation parameters have been optimized to achieve maximum energy efficiency and cost-effectiveness; and
- The economic feasibility and potential benefits of the suggested model have been assessed.

The present study holds significant importance for Aden, Yemen, as it pertains to developing and enhancing a hybrid solar-Rankine cycle configuration, incorporating thermal energy storage. The results of this research hold promise for offering a sustainable and effective remedy to the acute electricity deficit in Aden, Yemen. This solution could diminish the dependence on costly imported fuels and facilitate the area's economic growth. In addition, this initiative is expected to facilitate the incorporation of renewable energy sources and advance ecological sustainability in the region of Aden, Yemen.

1.6. OUTLİNE OF THE THESİS

The first chapter provides an overview of the current study, encompassing introductory information on solar energy, thermal energy storage, and various types of thermal energy storage, along with their respective benefits and drawbacks, as well as the primary objectives of the present work. Chapter Two comprehensively reviews the relevant literature related to the current investigation. In the third chapter of this thesis, the primary constituents and operational mechanisms of the proposed model are expounded upon. The third chapter moreover encompasses the input parameters that are fed into the system, as well as the thermodynamic and exergoeconomic equations that are employed in the energy, exergy, and economic analysis of the system. The fourth chapter of the work includes the results and discussion of the study. Chapter Five presents some concluding remarks and potential future endeavors.

CHAPTER TWO

LITERATURE REVIEW

The use of solar power plants combined with thermal energy storage has emerged as a possible solution to the intermittent nature of solar energy output. The integration of effective TES systems enables solar power plants to accumulate surplus energy during high solar irradiance periods and discharge it during periods of low or negligible sunlight, thereby ensuring a more uniform power output. Incorporating TES not only improves the dependability and adaptability of solar power facilities but also facilitates the expansion of renewable energy usage and the stability of the power grid. This literature review delves into the progress made in the domain of solar power plants that incorporate TES. It scrutinizes the diverse technologies, design factors, performance assessments, and possible applications.

Olivkar et al. [26] discussed using different materials for TES in solar thermal applications, including solar air heaters, solar dryers, and concentrated solar power plants. They discussed the performance and efficiency of various materials such as pebble stones, sand, metal chips, oil, gravel, cement, concrete, graphite, and recycled aluminum cans. The findings indicate that the utilization of sensible heat storage materials has the potential to enhance the thermal efficiency of solar air heaters, and solids have demonstrated potential for utilization in high-temperature heat storage applications compared to liquid.

Liu et al. [34] presented the design and optimization of TES systems for CSP plants, as seen in Figure 2.1. The study investigated different TES media, including phase change materials (PCMs) and solid sensible storage, and explored various storage configurations. The authors compared the performance of different TES systems and suggested that an economic analysis is necessary to select an optimal design. They also discussed various studies and experiments related to thermal energy storage

systems using PCMs for CSP plants. The research revealed that amalgamating metal/metal alloy phase change materials (PCMs) with salt PCMs in a cascade configuration could enhance energy density. However, the overall efficacy of the storage is only slightly enhanced. The research findings also indicated that using single graphite and PCM graphite-PCM sandwich TES configurations is feasible. However, these designs exhibit reduced energy density and necessitate increased storage material due to their limited operating temperature range. The hybrid design, which incorporates phase change materials (PCMs) with graphite, enhanced the graphite system's storage efficiency. Specifically, the storage effectiveness of the hybrid system was measured to be 80.2%, representing a significant improvement over the 59.0% storage effectiveness observed in the single graphite system.

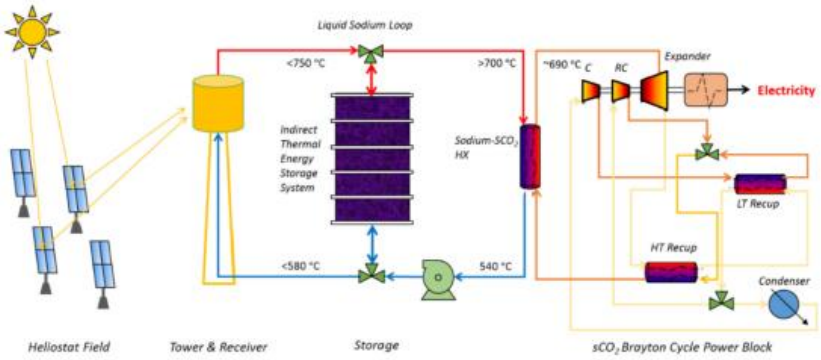

Figure 2. 1. A diagrammatic representation of a theoretical concentrated solar power (CSP) facility featuring a solar tower [34].

Mukherjee et al. [35] discussed different TES technologies and their application in concentrated solar thermal power plants. They compared two specific energy storage solutions, the TES System (TESS) and the Hydrogen Energy Storage System (HESS), and evaluated their performance in terms of capacity factors, energy and power density, efficiency, and other parameters. The findings indicate that TESS coupled with CSP can achieve a 100% capacity factor on a 24-hour scale. In comparison, the HESS can only achieve a capacity factor of approximately 58% due to its low round-trip efficiency. The round-trip efficiency of the TESS is notably higher at 98.45% in comparison to the HESS, which exhibits a significantly lower efficiency of approximately 33%. This discrepancy can be attributed to the presence

of multiple conversions in HESS, resulting in greater energy losses. Conversely, the TESS experiences solely heat losses as its primary form of energy loss.

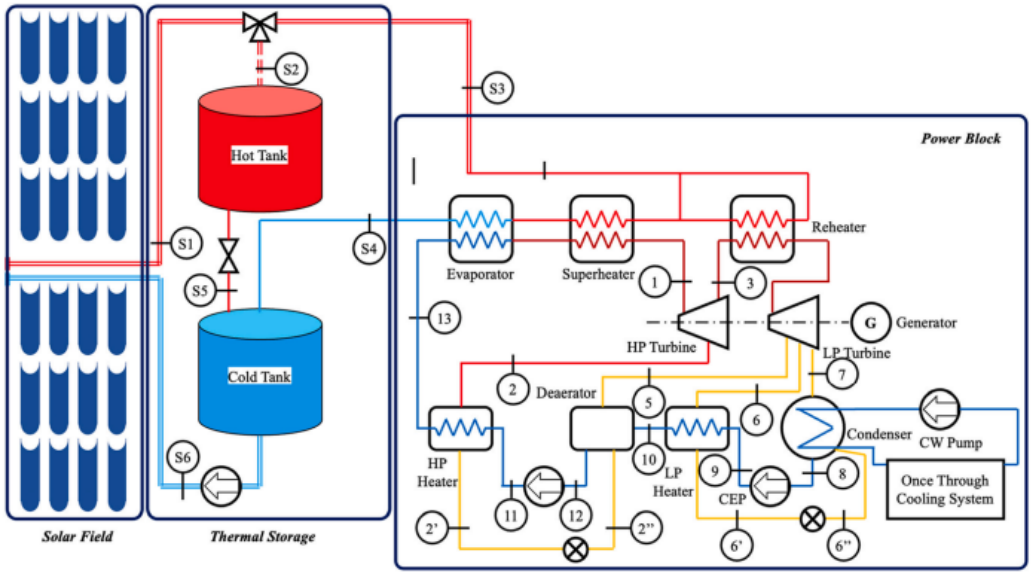

Figure 2. 2. Layout of CSP plant TESS [35].

Al-Qahtani [36] evaluated the performance of a Hybrid Solar Thermal Storage (HSTS) system proposed for CSP plants, as presented in Figure 2.3. The HSTS system uses a composite of PCM and a thermochemical storage (TCES) system encompassing paired metal hydride (MH) beds. The research conducted a comparative analysis of the operational efficacy of three distinct storage systems. These included a fundamental design utilizing solely TCES mode and two variations of the HSTS system, each featuring unique PCM heat exchanger designs.

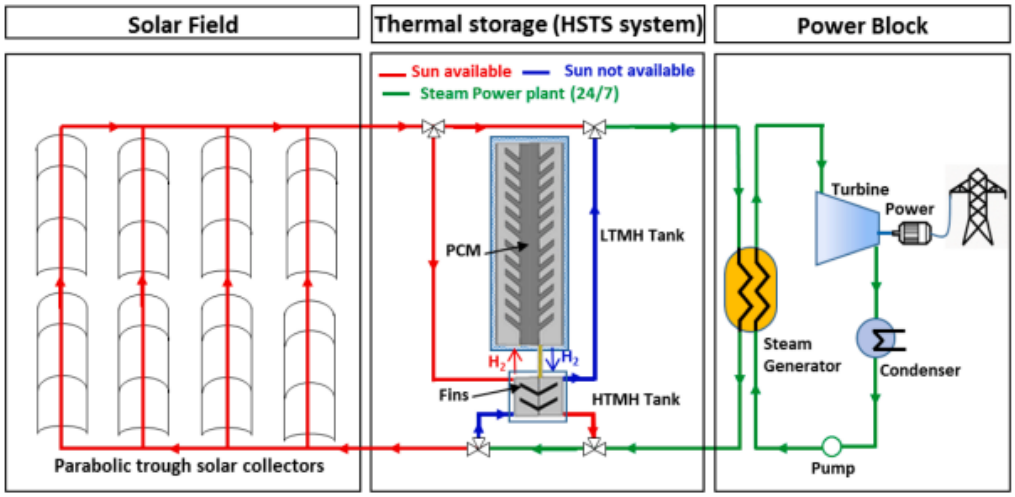

Figure 2. 3. Schematic of a CSP plant coupled with HSTS system [36].

Bouziane and Benhamou [37] introduced a study that evaluates the impact of different TES operation strategies on the performance of the PTC-CSP plant. The research used a computer model of a 55 MWe PT-CSP facility, comparable to the ANDASOL plant in Spain. The findings reveal that the proposed operating approach is effective in decreasing the plant's parasitic load and enhancing its overall efficiency. The recommended TES operating method is applicable on clear summer days with a long sunlight duration and a high solar elevation, but it is not applicable on clear days with a short sunlight period and a low solar elevation.

Qin et al. [38] investigated the technical and economic performance of different solar-assisted power generation (SAPG) system combinations with and without TES in three different locations with varying annual solar radiation. They studied the impact of a TES capacity and solar multiples (SM) on the specific cost of electricity and annual solar power output. The authors also compared their results with previous studies and provided insights into the optimal SAPG system configurations for different locations and operating conditions. The results showed that the technical advantage of different combinations of SAPG systems with and without TES decreases with the increase in solar multiple (SM) value. The utilization of the TES system has a significant influence on both the technical and economic aspects of the SAPG plant, thereby facilitating the enhancement of the annual solar-to-electricity (STE) efficiency and LCOE optimization of the SAPG plant.

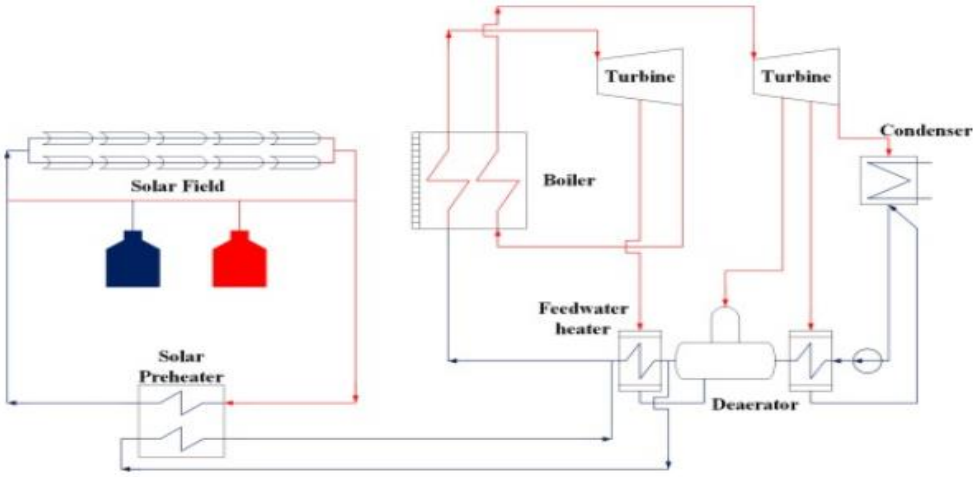

Figure 2. 4. Diagrammatic structure of a SAPG plant with TES system [38].

Luo et al. [39] examined the effects of solar multiple (SM) and thermal storage capacity on both the operational efficiency and economic evaluation of a dual-receiver solar power tower plant that is presented in Figure 2.5. The investigation employed a mathematical framework to compute the yearly efficacy of the plant, as well as a financial appraisal for varying SM and thermal storage capabilities. According to the findings of the study, the minimum levelized cost of electricity (LCOE) is 21.77 $/kWh. This was achieved through the implementation of an optimum SM of 1.7 and an optimum thermal storage capacity of 3 hours. The study provided insights into the optimal design and operational strategies for solar power tower plants. It also investigated the effects of optimal SMs, investment on the minimum LCOE, solar field equivalent electricity size, and thermal storage capacity.

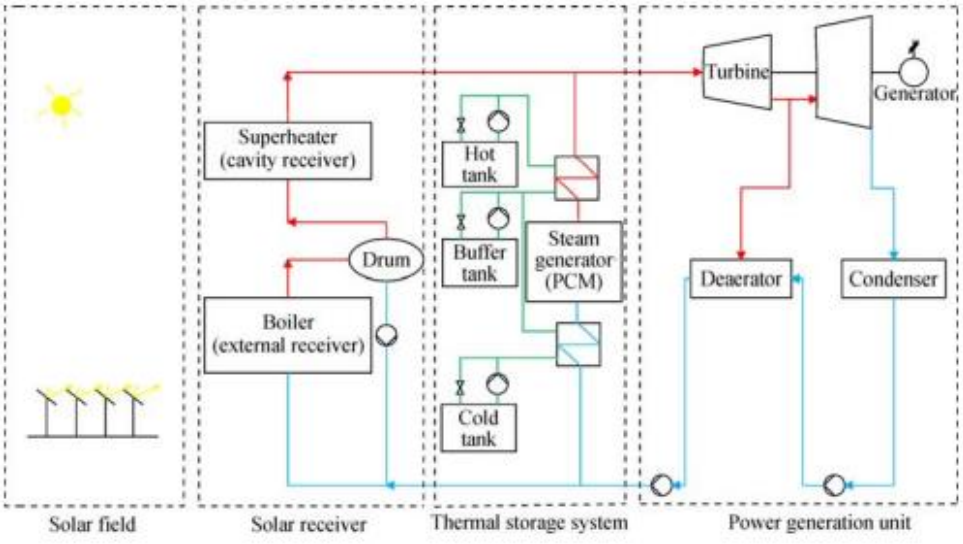

Figure 2. 5. Diagrammatic structure of DSG solar power tower plant [39].

Talal et al. [40] illustrated the potential for an integrated solar combined cycle (ISCC) in Iraq, which would combine solar thermal energy with gas turbine technology. The authors discussed various studies and analyses related to ISCC systems, covering topics such as thermodynamic and economic analysis, performance evaluation, and optimization. The results showed that integrating solar thermal fields with a natural gas combined cycle (NGCC) is both economically and thermodynamically feasible, with the ISCC system performing better than the NGCC system in terms of energy and exergy efficiencies. The research underscored the significance of broadening the scope of Iraq's electricity infrastructure by integrating sustainable energy sources. It recommended the establishment of an ISCC plant in Mosul, Iraq.

Jiang et al. [41] investigated a tower solar-aided coal-fired power generation system (TSACPG) that incorporates thermal energy storage. The system integrated solar energy with a coal-fired power plant to increase efficiency and reduce CO_2 emissions. The study included simulations and an economic analysis to determine the optimal TES capacity and heliostat field area for different typical days and DNI levels. The findings indicate that the implementation of the TSACPG technology can significantly mitigate CO_2 emissions and confer economic benefits in comparison to the utilization of solely coal-fired power generation. The incorporation of solar

energy into the TSACPG system has the potential to enhance the exergy efficiencies of the boiler and decrease the rates of standard coal consumption.

Liu et al. [42] introduced a summary of different studies related to TES systems for CSP plants. The studies investigated different TES configurations and materials and analyzed the impact of system size, tube size, and hot HTF temperatures on cost and performance. The studies also included economic models to calculate the cost of the TES systems under investigation and identified potential design enhancements to reduce materials and costs.

Khamlich [43] evaluated the technical and economic feasibility of different TES configurations in a 100 MW CSP plant with 8 hours of TES capacity. The research examined five different TES models and employed the net present value (NPV) to assess economic viability. The findings indicate that the single-tank thermocline storage and latent heat storage technologies exhibited superior economic feasibility compared to other technologies. Conversely, the two-tank indirect sensible heat storage technology demonstrated lower financial gains due to the utilization of costly heat transfer fluid materials. The authors highlighted the significance of implementing production optimization techniques that are based on a price-driven approach in order to enhance the profitability of Concentrated Solar Power (CSP) plants.

Ehsan et al. [44] evaluated the performance of a dry-cooled CSP plant with a supercritical CO_2 power cycle and TES, as seen in Figure 2.6. This study focuses on examining the dynamic behavior of a plant in response to fluctuations in both solar insulation and ambient temperature. The article covered the selection of hot salt and cold tank temperatures, the sizing of the heliostat field, and the sizing of the cooling tower, and the evaluation of tank capacity. The authors provided a comprehensive review of various studies on supercritical carbon dioxide (sCO_2) power cycles for CSP plants and discussed the challenges and opportunities for the commercialization of sCO_2 power cycles in the renewable energy sector.

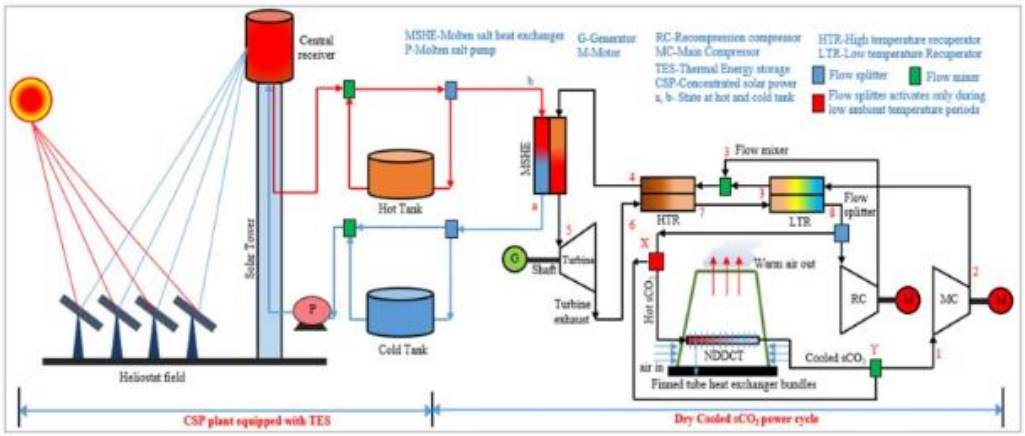

Figure 2. 6. A diagram of a dry cooled sCO_2 CSP plant with TES [44].

Chen et al. [45] investigated the optimal sizing of STP plants with TES. The study analyzed the optimal design parameters for a 50 MW STP plant based on a steam Rankine cycle (RC) with a molten salt storage system. The impacts of design direct normal irradiance (DNI), solar multiple (SM), and TES hours on the levelized cost of electricity (LCOE) and the capacity factor are analyzed. The findings indicate that the ideal configuration of DNI is contingent upon the yearly quantity of radiation and the dispersion of solar irradiance, which deviates from the suggested benchmarks derived from conventional approaches. The TES system positively affects the system's capacity factor and its annual electricity generation. The findings presented in this study have the potential to enhance comprehension of the interplay between crucial design parameters and facilitate the identification of the most advantageous design for STP systems across varying solar resources.

d'Entremont et al. [46] conducted a simulation of a bench-scale metal hydride (MH) system intended for TES in a CSP, as presented in Figure 2.7. The MH materials employed, the desorption and absorption kinetics, and the system modelling were explained by the authors. The findings demonstrate the temperature and pressure patterns of the metal hydride (MH) beds during their charging and discharging processes. The implications of these outcomes for the enhancement and configuration of more extensive MH systems are analyzed in the study. The performance of a paired-metal hydride TES system was simulated using two different metal hydrides, $TiCr_{1.6}Mn_{0.2}$ and $NaMgH_2F$, and the effects of enhanced

thermal conductivity were examined. The findings indicated that paired-metal hydride configurations exhibit promising prospects for implementation in TES applications.

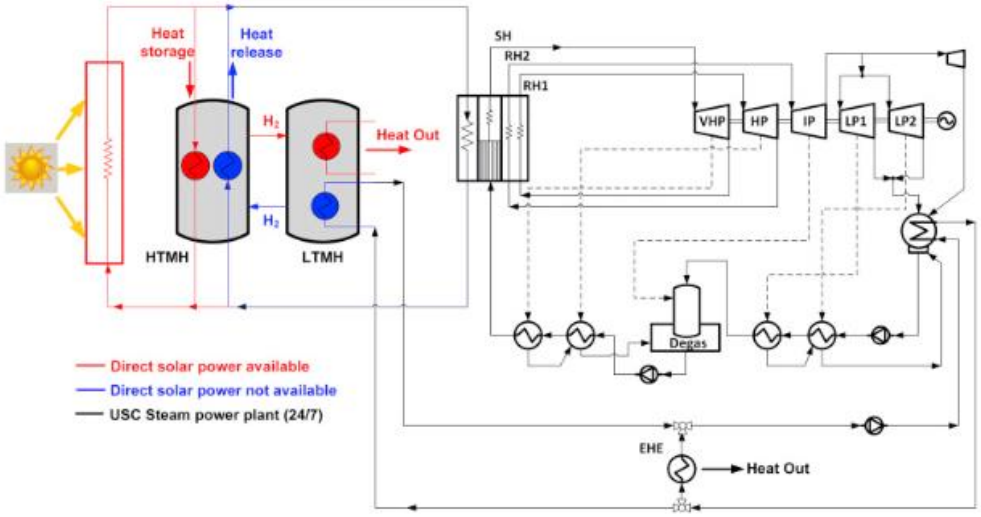

Figure 2. 7. Solar-powered USC steam plant with MH-based TES system [46].

The utilization of various TES systems for CSP plants, particularly for direct steam generation (DSG) in solar power plants, was investigated by Prieto et al. [47]. The research conducted a comparative analysis of three distinct TES alternatives, namely molten salts, steam accumulators, and phase change materials, with a focus on assessing their efficacy and economic feasibility. The research findings suggest that the optimal TES alternative is contingent upon the storage system's discharge capacity, as certain alternatives may prove more beneficial for varying storage durations. The investigation also scrutinized the cost sensitivity of TES systems and concluded that prioritizing the reduction of accumulator system costs over the reduction of molten salt system costs would be advisable.

In a study conducted by Ciani Bassett et al. [48], a hybrid geothermal-solar power plant (GSPP) was modeled, incorporating a TES unit to enhance the utilization of geothermal energy and optimize the performance of the organic Rankine cycle system. The authors highlighted examples of hybridization strategies, such as the still water power plant, and expounded upon the design and off-design models of the geothermal power plant. The study presented a detailed design and off-design model

of a hybrid GSPP, consisting of a PTC solar field and an air-cooled binary cycle geothermal plant. The findings indicate that incorporating a solar system into a geothermal power plant maintains the geothermal fluid's temperature near the intended level, consequently guaranteeing an elevated thermal efficiency of the ORC system. The implementation of a TES system enables the optimization of solar energy generation through the transfer of surplus solar energy production from daytime to nighttime periods, characterized by lower ambient temperatures and higher power system efficiency. The finding revealed that the TES system alone led to a 19% increase in the productivity of the solar section.

Peiró et al. [49] investigated the pilot plant's design, start-up, and operation of a two-tank molten salt TES system intended for the CSP plant. The authors presented their insights and suggestions for enhancing the design and functioning of these power plants. These recommendations encompass various aspects such as ensuring the compatibility of materials, accurate operation of instrumentation, and effective operational process strategies. In addition, the authors provided suggestions for preventing malfunctions, and underscored the significance of the appropriate installation of electrical heat tracing and insulation.

Pelay et al. [50] reviewed the various aspects of TES systems in CSP plants. The various TES technologies, the current advancements in CSP plants, and the principles for their assimilation into CSP plants were discussed. The authors of the study arrived at the conclusion that the implementation of TES systems is imperative for enhancing the dispatchability and economic competitiveness of forthcoming high-capacity CSP plants.

Andika et al. [51] investigated the evaluation of the technological and economic potential for improving TES systems for CSP plants. The study considered various factors such as temperature, materials, and costs to determine the most efficient TES system. The findings indicate that selecting materials for thermal energy storage (TES) only sometimes ensures a reduction in the specific cost of electricity. The study's results also indicated that there is a possibility for enhancements in TES for CSP systems.

Adibhatla et al. [52] analyzed the potential economic and environmental advantages that could be derived from integrating solar energy with conventional coal-fired thermal power plants. The study also examined the feasibility of implementing solar-aided feed water heating (SAFWH) in a 500 MW sub-critical thermal power plant located in India, with a focus on its performance and economic viability. The research findings suggest that investigating alternative sources of energy, specifically solar power, is a viable option given the depleting reserves of non-renewable fossil fuels and the escalating costs associated with them. The results proved that integrating solar thermal energy into a 500 MWe subcritical coal-fired power plant through SAFWH can significantly improve energy efficiency and fuel savings and reduce coal, CO_2, and ash emissions. The utilization of solar energy in lieu of a turbine bleed stream for high-pressure feed water heater led to a 5-6% enhancement in coal consumption and an increase in power generation. The solar-aided option with TES has the highest fuel savings and plant efficiency, and also the highest capital costs.

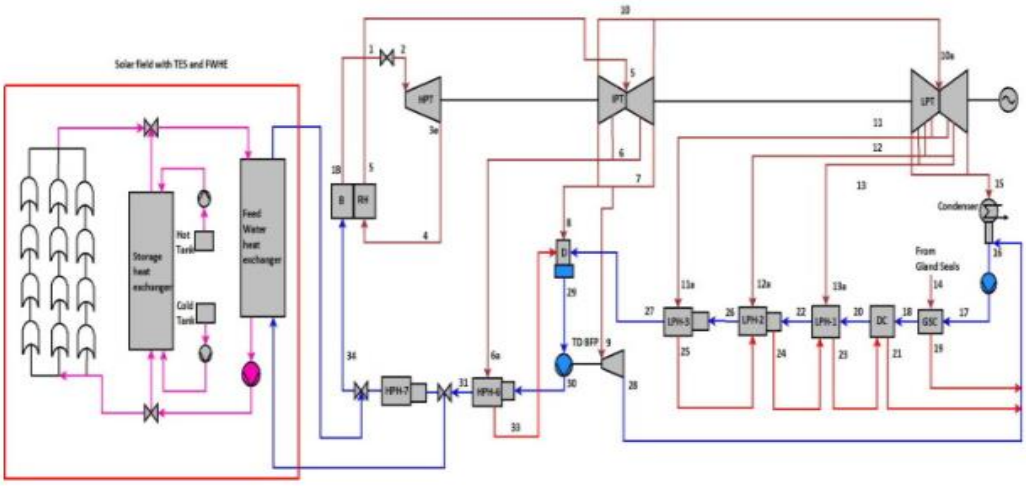

Figure 2. 8. Schematic of 500 MWe TPP incorporated with SAFWH in HPH-7 [52].

Pizzolato et al. [53] introduced a summary of different articles related to CSP plants with TES and cogeneration capabilities. The study discussed the modeling, optimization, and experimental validation of various CSP plant designs with integrated steam generators and single-tank thermal energy storage systems. The results of the different articles summarized in this document showed that CSP plants with TES and cogeneration capabilities have the potential to generate electricity at a

lower cost and provide heat for various applications. The authors also suggested that the single-tank TES system with an integrated steam generator is more cost-effective than the double-tank option. The optimization of the CSP plant design led to better energetic and economic performance, and the use of genetic algorithms helped in achieving the optimal design. The authors also highlighted the potential of CSP technology for mid-size industrial users and the competitiveness of the technology in specific markets with real thermal users. However, more research and development are needed to overcome technical and economic challenges.

Grange et al. [54] investigated the influence of TES integration on the efficacy of a hybrid solar-gas turbine power plant. The research has demonstrated that the incorporation of a TES system results in enhanced and consistent electricity generation, elevated daily mean solar fraction of the power station, and a rise in electrical output per unit of fuel utilized.

Rodríguez et al. [55] established a performance model for a CSP plant with a TES system. They also compared different TES systems for a 1 MW CSP plant with an ORC power block and concluded with a financial analysis of the different TES systems. The findings indicated that there is no significant difference in the additional solar energy captured among all TES layouts. However, it was observed that thermocline systems exhibit considerably lower capital investment costs. The research also revealed that indirect systems incur higher costs compared to direct systems. Additionally, augmenting the storage capacity of the plant is advantageous as it leads to a rise in electricity generation and a reduction in overall energy wastage, thereby enhancing global efficiency. The study concluded with a financial analysis of different TES systems.

Chacartegui et al. [56] provided a comprehensive examination of a solar thermal power plant's design, analysis, and economic evaluation utilizing Organic Rankine Cycle (ORC) technology. The research also included an economic model for calculating the levelized energy cost and specific cost of electricity for the proposed plant. The study evaluated the performance of different working fluids and thermal energy storage configurations and examines the costs and benefits of using CSP

plants, specifically PTCs, for electricity generation. The findings indicated that toluene and cyclohexane exhibit optimal performance as working fluids in the ORC system. Additionally, the direct TES configuration is more economically viable than the indirect configuration.

Casati et al. [57] evaluated the possibility of using optimal control techniques to boost the profitability of CSP plants with a TES. The study conducted a comparative analysis of various operational approaches through an in-depth financial evaluation throughout the duration of the project. The findings indicated that incorporating optimal control into the plant's design and sizing phase is crucial for accurately estimating its potential revenue. The investigation also unveiled the potential of optimal control to diminish investment expenses by achieving equivalent revenue with a reduced storage capacity.

CHAPTER THREE

MODELING OF THE COMBINED SOLAR-RC WITH A THERMAL ENERGY STORAGE UNIT

3.1. MODEL DESCRIPTION

The schematic of the Rankine cycle driven by parabolic trough solar collectors and thermal energy storage will be examined in this chapter. As seen in Figure 3.1, the integrated system proposed in this thesis consists of parabolic trough solar collectors (PTCs), a thermal storage unit, and a Rankine cycle, respectively. PTCs are responsible for heating the working fluid by capturing solar irradiation and converting it to thermal energy. In the collector field circuit and the storage tank, molten salt serves as the working fluid. The next component of the system is the storage tank. Cold molten salt exits the lower half of the storage tank and enters the collector field, where its temperature rises before returning to the upper part of the storage tank. On the other side of the tank, hot molten salt moves from the top of the storage tank to the boiler to heat the working fluid of the RC. The colder molten salt flows back to the bottom of the storage tank, closing the molten salt circuit. Finally, the Rankine steam cycle is powered by the hot molten salt from the thermal storage tank.

A thermodynamic analysis of the integrated solar-RC with a thermal energy storage unit was performed using the Engineering Equations Solver (EES) program, within certain assumptions, using the First and Second Laws of Thermodynamics, and general energy, exergy, and cost equations.

Thermodynamic and thermoeconomic assessments for the proposed system are based on the following presumptions:

- There is no heat loss from the system to the environment, and the pressure drop is negligible;
- The pressure (P_0) and the temperature (T_0) at the reference state are 1 bar and 25℃, respectively;
- The energies, both kinetic and potential, are fixed;
- The system's steady-state operating conditions are considered;
- The compressor, pump, and turbines operate in an adiabatic process; and
- The sun's temperature is estimated to be 6,000 K.

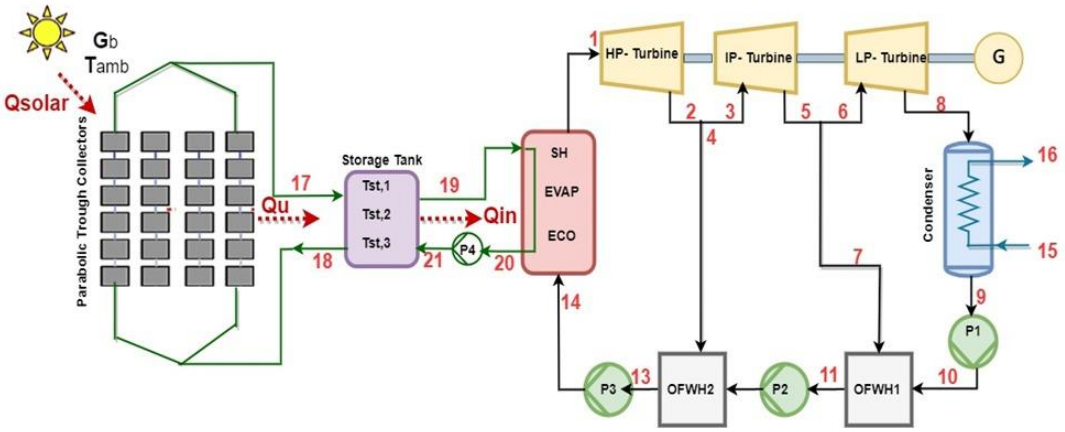

Figure 3. 1. Flowsheet of the integrated solar- RC with a thermal energy storage unit.

In addition, to show the system's accuracy, the values of a study in the literature were calculated with the expressions used in the design. The results obtained are compared in Table 3.1. When the obtained results were examined, it was seen that the values were close to each other. From these results, the correctness of the solution path of the system has been proven.

Table 3. 1. Comparison of the values calculated in the literature with the values in this study.

Parameter	Thesis	Reference [58]	Difference
HPT inlet pressure	100000 Pa	100000 Pa	0%
Condenser pressure	8428 Pa	8484 Pa	0.66%
Steam mass flow rate	23.7 kg/s	23.67 kg/s	0.12%
Net power output	20.4 MW	20 MW	1.96%
Rankine cycle efficiency	33.8%	33%	2.5%
Required thermal energy	60.35 MW	60 MW	0.6%
HTF at inlet of boiler	565°C	565°C	0%
HTF at exit of boiler	286°C	286°C	0%
HTF mass flow rate	141 kg/s	141 kg/s	0%

3.2. THERMODYNAMIC ANALYSIS

Each component in the integrated solar-RC with thermal energy storage is thermodynamically modeled separately. In the proposed system, equations were created for mass, energy, exergy, and energy-economic analyses. Table 1 lists the operational and technical parameters used in the analysis.

Table 3. 2. Summary of design point parameters.

Parameter	Value	Unit
Ambient temperature	28.7	°C
Latitude location	12.7855	° N
Longitude	45.0187	° E
Plant location	Aden/ Yemen	-
Average DNI	6.14	kWh/ m2. day
Solar field area	510120	m2
PTC working fluid	Molten salt	-
Boiler pinch temperature	10	°C
HPT inlet pressure	150	bar
IPT inlet pressure	45	bar
LPT inlet pressure	10	bar
Condenser temperature	50	°C
Turbine isentropic efficiency	85	%
Pump isentropic efficiency	80	%
HPT extraction ratio	0.2	-
LPT extraction ratio	0.15	-

3.3. ENERGY AND EXERGY ANALYSIS OF THE SYSTEM

The mass, energy, and exergy equations of the system are written separately for the general system and each component. In a continuous flow open system, the total mass in the control volume does not change with time. In this case, according to the principle of conservation of mass, the total mass entering the control volume must be equal to the total mass leaving the control volume. In addition, for a continuous flow open system, the mass flowing per unit time or the mass flow rate m (in kg/s) gains importance rather than the mass entering and exiting the system over a period of time. Accordingly, for a generally continuous flow system with multiple inlets and outlets, the principle of conservation of mass is as follows:

$$\sum \dot{m}_{in} = \sum \dot{m}_{out} \quad (3\text{-}1)$$

In continuous flow open systems, the total energy in the control volume is constant (E_{cv} = constant). Thus, the total energy change in the control volume is zero ($\Delta E_{cv} = 0$). Therefore, the amount of energy entering the control volume is equal to the amount of energy leaving the control volume. The following equations give the principle of conservation of energy for a continuous flow open system [59,60]:

$$\sum \dot{E}_{in} = \sum \dot{E}_{out} \quad (3\text{-}2)$$

$$\dot{Q}_{in} + \dot{W}_{in} + \sum \dot{m}_{in} h_{\text{in}} = \dot{Q}_{out} + \dot{W}_{out} + \sum \dot{m}_{out} h_{out} \quad (3\text{-}3)$$

According to the heat input transferred to the system and the work produced by the system, the First Law of Thermodynamics or the conservation of energy relation for an open system with continuous flow is expressed by the following equation [59,61]:

$$\dot{Q} + \dot{W} = \sum \dot{m}_{out} h_{out} - \sum \dot{m}_{in} h_{\text{in}} \quad (3\text{-}4)$$

Exergy ensures more effective use and protection of energy resources. It also helps to make the First and Second Laws of Thermodynamics more understandable. The importance of exergy analysis can be listed as follows:

- It is the main tool in determining the environmental impact of using energy resources in the best way;
- It is an efficient method for designing and analyzing energy systems, using the principles of conservation of mass and energy together with the second law of thermodynamics;
- It shows how designing more efficient energy systems is possible by reducing the inefficiencies and losses in actively used systems;
- It plays a key role in sustainable, high-efficiency environmental energy production; and
- It helps countries and global companies to develop a more effective energy strategy and policy.

With the Second Law of Thermodynamics, the quality of energy gains importance as well as its quantity. Energy analysis does not provide any information about the irreversibility of a thermodynamic process. However, the exergy analysis of the system provides insight into the inefficiencies in the design and offers opportunities to minimize the exergy loss of thermodynamic processes. The general exergy balance of the system can be written as [62]:

$$\sum(\dot{m}ex)_{in} + \dot{E}x_{in,W} + \dot{E}x_{in,Q} = \sum(\dot{m}ex)_{out} + \dot{E}x_{\text{out},W} + \dot{E}x_{\text{out},Q} \quad 3\text{-}5$$

$$\dot{E}x_Q = \dot{Q}\left(1 - \frac{T_0}{T_s}\right) \quad 3\text{-}6$$

$$\dot{m}_{\text{in}} S_{\text{in}} + \left(\frac{\dot{Q}}{T}\right) + \dot{S}_{\text{gen}} = \dot{m}_{\text{out}} S_{\text{out}} \quad 3\text{-}7$$

The energy equations for the parabolic solar collector are given below [58, 59]. These equations should consider two types of energy (heat energy). One is the solar energy input ($\dot{Q}_{\text{Solar}}$) obtained from the total sun, and the other is the heat transfer to the system and is expressed as useful solar energy ($\dot{Q}_{\text{u}}$). These energies are calculated as in the following equations [40]:

$$\dot{Q}_{\text{Solar}} = A_A \cdot F_R \cdot \text{S} \cdot n_{cp} n_{cs} \quad 3\text{-}8$$

$$\dot{Q}_u = n_{cp} n_{cs} F_R [S A_a - A_r U_L (T_{ri} - T_o)] \quad 3\text{-}9$$

In these equations n_{cp}, n_{cs}, A_a, and A_r are the number of collectors in series and in parallel, the aperture and receiver areas in the parabolic solar collector, respectively. F_R, S and U_L represent the collector heat gain factor, the amount of absorbed solar radiation and the heat loss coefficient of the collector and are calculated with the following equations:

$$F_R = \frac{\dot{m}_c C_{p,c}}{A_r U_L}\left[1 - \exp\left(-\frac{U_L F' A_r}{\dot{m}_c C_{p,c}}\right)\right] \quad 3\text{-}10$$

$$\text{S} = DNI \cdot q_{PTC} \cdot \gamma \cdot \tau \cdot \alpha \cdot \text{K} \quad 3\text{-}11$$

$$F' = \frac{1/U_L}{\frac{1}{U_L} + \frac{D_{o,r}}{h_f D_{i,r}} + \left(\frac{D_{o,r}}{2k} \ln \frac{D_{0,r}}{D_i, r}\right)} \quad 3\text{-}12$$

$$U_L = \left(\frac{A_R}{(h_w + h_{rc}) \cdot A_G} + \frac{1}{h_{rr}}\right)^{-1} \quad 3\text{-}13$$

$$\dot{E}x_{Q,Solar} = \dot{Q}_{solar}\left(1 - \frac{T_0}{T_{PTC}}\right) \quad 3\text{-}14$$

While the exergy entering the system with solar radiation is calculated from the above formulas, the total solar collector area can be calculated from the equation below [65]:

$$A_a = \dot{Q}_{solar}(w - D_{a,r})L \quad 3\text{-}15$$

The thermodynamic model created for the thermal energy storage tank calculations is as follows. To calculate the heat loss from the thermal energy storage tank in the system to the environment, firstly, the total heat loss coefficient (*U*) is calculated, and then the total heat loss is calculated with Equations 3-17 [66,67].

$$\frac{1}{U} = \frac{1}{h} + \frac{l}{k} \quad 3\text{-}16$$

where h is the heat transfer coefficient (in W/m^2 K), k the conductivity heat transfer (in W/m K), and l the insulation thickness used around the tank [68–70]

$$\dot{Q}_{HST,\,\text{lostc}} = U^*(T_{HST} - T_0)^* A \quad 3\text{-}17$$

where A is the total tank surface area (in m^2), T_{HST} the protection available in the tank, and T_o the environmental protection (in ℃). There are three different operating modes in the thermal energy storage tank, namely those of charging, discharging and storage. The total amount of energy stored throughout the charge is calculated using the following equations [62, 63]:

$$\dot{Q}_{HST} = \dot{Q}_u - \dot{Q}_{HST,\,\text{lostc}} \quad (3\text{-}18)$$

$$\sum Q_{HST} = \dot{Q}_{HST} * \Delta t_h \quad (3\text{-}19)$$

where Δt_h is the charging time. The temperature of the storage tank (T_{HST}) is found with the following equation [68]:

$$T_{HST} = \frac{\sum Q_{HST}}{c_{p,HST} * M_{HST}} \quad (3\text{-}20)$$

where M_{HST} is the total amount of fluid in the tank. The following equations are used for the variation of the tank temperature during the storage phase and the total heat loss calculations during the storage period [62, 64]:

$$T_{HST}^{+} = T_{HST} + \frac{\Delta t_h}{M_{HST} * c_{p,HST}}[-UA(T_{HST} - T_0)] \quad (3\text{-}21)$$

$$Q_{HST,losss} = M_{HST} * c_{p,HST} * (T_{HST} - T_{HST}^{+}) \quad (3\text{-}22)$$

The heat transferred to the generation system during the discharge period is calculated as follows [68,69]:

$$Q_{HST,\,\text{disharged}} = \sum Q_{HST} - Q_{HST,\,\text{losts}} \quad (3\text{-}23)$$

The energy and exergy equations for the components used in the system are shown in Table 4.3. Fuel and product exergy for each component are shown in Table 4.4. The energy and exergy efficiency of the overall system are calculated from the following equations.

The power consumed in the pumps is found with the following equations [72–74]:

$$\eta_{Pump} = \frac{\dot{W}_{Pump,ideal}}{\dot{W}_{pump,actual}} \quad (3\text{-}24)$$

$$\dot{W}_{pump,ideal} = v * (P_{\text{out}} - P_{\text{in}}) \quad (3\text{-}25)$$

The power produced in the steam turbine is found with the following equations:

$$\eta_{ST} = \frac{\dot{W}_{ST,actual}}{\dot{W}_{ST,ideal}} \quad 3\text{-}26$$

$$\dot{W}_{ST,ideal} = \dot{m}_{ST,in} * \left(h_{ST,\,\text{in}} - h_{ST,\,\text{out}}\right) \quad 3\text{-}27$$

$$\dot{W}_{net} = \eta_{GEN} * \left(\dot{W}_{ST} - \dot{W}_{Pump}\right) \quad 3\text{-}28$$

The First and Second Law efficiencies of the triple combined cycle can be determined as follows [59,75]:

$$\eta_{\text{I}} = \frac{\dot{W}_{\text{net}}}{\dot{Q}_{\text{in}}} \quad 3\text{-}29$$

$$\eta_{\text{II}} = \frac{\dot{W}_{\text{net}}}{\dot{E}x_{in}} \quad 3\text{-}30$$

The power output from the triple combined system can be found thus:

$$\dot{W}_{\text{net}} = \dot{W}_{\text{HPT}} + \dot{W}_{\text{IPT}} + \dot{W}_{\text{LPT}} - \dot{W}_{\text{Pump1}} - \dot{W}_{\text{Pump2}} - \dot{W}_{\text{Pump3}} \quad 3\text{-}31$$

The system's heat and exergy input can be determined as follows:

$$\dot{Q}_{in} = \dot{Q}_{\text{Solar}} \quad 3\text{-}32$$

$$\dot{E}x_{in} = \dot{E}x_{Q,Solar} \quad 3\text{-}33$$

Table 3. 3. Energy and exergy balance equations in the triple-cycle power plant

Component	Energy balance equation	Exergy balance equation
HPT	$\dot{m}_1 h_1 = \dot{m}_2 h_2 + \dot{W}_{HPT}$	$\dot{E}x_{D,HPT} = \left(\dot{E}x_1 - \dot{E}x_2\right) - \dot{W}_{HPT}$
IPT	$\dot{m}_3 h_3 = \dot{m}_5 h_5 + \dot{W}_{IPT}$	$\dot{E}x_{D,IPT} = \left(\dot{E}x_3 - \dot{E}x_5\right) - \dot{W}_{IPT}$
LPT	$\dot{m}_6 h_6 = \dot{m}_8 h_8 + \dot{W}_{LPT}$	$\dot{E}x_{D,LPT} = \left(\dot{E}x_6 - \dot{E}x_8\right) - \dot{W}_{LPT}$
Condenser	$\dot{m}_8(h_8 - h_9) = \dot{m}_{15}(h_{16} - h_{15})$	$\dot{E}x_{\mathrm{D,cond}} = \dot{E}x_8 - \dot{E}x_9 + \dot{E}x_{15} - \dot{E}x_{16}$
Pump1	$\dot{m}_9\, h_9 + \dot{W}_{pump1} = \dot{m}_{10}\, h_{10}$	$\dot{E}x_{D,pump1} = \left(\dot{E}x_9 - \dot{E}x_{10}\right) + \dot{W}_{pump1}$
OFWH1	$\dot{m}_7 h_7 + \dot{m}_{10} h_{10} = \dot{m}_{11} h_{11}$	$\dot{E}x_{D,OFWH1} = \dot{E}x_7 + \dot{E}x_{10} - \dot{E}x_{11}$
Pump2	$\dot{m}_{11}\, h_{11} + \dot{W}_{pump2} = \dot{m}_{12}\, h_{12}$	$\dot{E}x_{D,pump2} = \left(\dot{E}x_{11} - \dot{E}x_{12}\right) + \dot{W}_{pump2}$
OFWH2	$\dot{m}_4 h_4 + \dot{m}_{12} h_{12} = \dot{m}_{13} h_{13}$	$\dot{E}x_{D,OFWH2} = \dot{E}x_4 + \dot{E}x_{12} - \dot{E}x_{13}$
Pump3	$\dot{m}_{13}\, h_{13} + \dot{W}_{pump3} = \dot{m}_{14}\, h_{14}$	$\dot{E}x_{D,pump3} = \left(\dot{E}x_{13} - \dot{E}x_{14}\right) + \dot{W}_{pump3}$
Boiler	$\dot{m}_1(h_1 - h_{14}) = \dot{m}_{19}(h_{19} - h_{20})$	$\dot{E}x_{\mathrm{D,Boiler}} = \dot{E}x_{14} - \dot{E}x_1 + \dot{E}x_{19} - \dot{E}x_{20}$
Storage tank	$\dot{m}_{17}(h_{17} - h_{18}) = \dot{m}_{19}(h_{19} - h_{21}) + UA(T_{19} - T_{\mathrm{amb}})$	$\dot{E}x_{\mathrm{D,TES}} = \dot{E}x_{17} - \dot{E}x_{18} + \dot{E}x_{19} - \dot{E}x_{21}$
Pump4	$\dot{m}_{20}\, h_{20} + \dot{W}_{pump4} = \dot{m}_{21}\, h_{21}$	$\dot{E}x_{D,pump4} = \left(\dot{E}x_{20} - \dot{E}x_{21}\right) + \dot{W}_{pump4}$
PTC	$\dot{m}_{18} h_{18} + \dot{Q}_u = \dot{m}_{19}\, h_{19}$	$\dot{E}x_{D,PTC} = \left(\dot{E}x_{18} - \dot{E}x_{19}\right) + \dot{E}x_{Q,Solar}$

Table 3. 4 Product and fuel exergy equations

Component	Fuel exergy equation	Product exergy equation
HPT	$\dot{E}x_1 - \dot{E}x_2$	$\dot{W}_{HPT}$
IPT	$\dot{E}x_3 - \dot{E}x_5$	$\dot{W}_{IPT}$
LPT	$\dot{E}x_6 - \dot{E}x_8$	$\dot{W}_{LPT}$
Condenser	$\dot{E}x_8 - \dot{E}x_9$	$\dot{E}x_{16} - \dot{E}x_{15}$
Pump1	$\dot{W}_{pump1}$	$\dot{E}x_{10} - \dot{E}x_9$
OFWH1	$\dot{E}x_7 + \dot{E}x_{10}$	$\dot{E}x_{11}$
Pump2	$\dot{W}_{pump2}$	$\dot{E}x_{12} - \dot{E}x_{11}$
OFWH2	$\dot{E}x_4 + \dot{E}x_{12}$	$\dot{E}x_{13}$
Pump3	$\dot{W}_{pump3}$	$\dot{E}_{14} - \dot{E}_{13}$
Boiler	$\dot{E}x_{19} - \dot{E}x_{20}$	$\dot{E}x_1 - \dot{E}x_{14}$
Storage tank	$\dot{E}x_{17} - \dot{E}x_{18}$	$\dot{E}x_{19} - \dot{E}x_{21}$
PTC	$\dot{E}x_{Q.Solar}$	$\dot{E}x_{18} - \dot{E}x_{17}$

3.4. THERMOECONOMIC ANALYSIS (SPECO METHOD)

When the concept of exergy is combined with the principles of engineering economics, the result is known as thermoeconomics, or exergoeconomics. Thermoeconomics defines the real cost sources at the component level. These costs are capital investment costs, operating and maintenance costs, and costs associated with the destruction or loss of exergy. The optimization of thermal systems is achieved by considering such cost sources [76].

Thermoeconomics is an exergy-assisted cost reduction method that combines exergy and cost analysis [77]. Exergoeconomics also includes the interconnections between thermodynamics and economics and understanding the behaviors of an energy conversion plant in terms of cost. In particular, exergy destruction and exergy losses are evaluated to determine the thermodynamic inefficiencies of these systems. Knowing the costs of such inefficiencies is very useful to increase the economic efficiency of the system, that is, to reduce the costs of the final products produced by the system [78,79].

The general exergy-cost balance equation for each component in the system can be written as follows [80,81]:

$$\sum \dot{C}_{P,k} = \sum \dot{C}_{F,k} + Z_k^{CI} + Z_k^{OM} \qquad 3\text{-}34$$

In the above equation, $\dot{C}_P$ is the cost ratio associated with the product of the system, $\dot{C}_F$ is the ratio of the total expenditure to produce the product, that is, the fuel cost ratio, Z^{CL} the initial investment cost of the system, and Z^{OM} the cost associated with the operation, maintenance and repair of the system. The average unit exergy cost for each flow is calculated with the following equation [78]:

$$c_i = \frac{\dot{C}_i}{\dot{E}x} \qquad 3\text{-}35$$

$\dot{C}$ is expressed in \$/h, and c in \$/GJ. When Equation 3.35 is written as a product exergy ratio and a fuel exergy ratio, the following equation is obtained [82]:

$$c_p \dot{E}x_{p,k} = c_f \dot{E}x_{D,k} + \dot{Z}_k \quad 3\text{-}36$$

Here, $\dot{Z}_k$ is the sum of the variables Z^{CL} and Z^{OM} given in Equation 3.34. In exergy costing, a cost rate is associated with each exergy transfer. Exergy transfer of the incoming and outgoing flows ($\dot{E}x_f$ and $\dot{E}x_p$), power $(\dot{W})$ and exergy are associated with heat transfer $(\dot{E}x_q)$. The exergy costs that occur with the exergy flow entering and leaving the system, power and heat transfer are calculated with the following equations [83]:

$$\dot{C}_f = c_f \dot{E}x_f \quad 3\text{-}37$$

$$\dot{C}_p = c_p \dot{E}x_p \quad 3\text{-}38$$

$$\dot{C}_q = c_q \dot{E}x_q \quad 3\text{-}39$$

$$\dot{C}_w = c_w \dot{W} \quad 3\text{-}40$$

In these equations, c_f, c_p, c_w, and c_q represent the unit cost of the input flow, output flow, work and heat, respectively. The exergy cost balance equation for each component of the system is written as follows [80][84]:

$$\sum \dot{C}_{in,k} + \dot{C}_{Q,k} + \dot{Z}_k = \sum \dot{C}_{out,k} + \dot{C}_{w,k} \quad 3\text{-}41$$

$\dot{C}_{Q,k}$, and $\dot{C}_{w,k}$ are the heat and power exergy cost flow, respectively, and $\dot{Z}_k$ is the capital cost, operation and maintenance cost flow, which is calculated from the formula below [78]:

$$\dot{Z}_k = PEC_k * CRF * \frac{\phi}{t} \quad 3\text{-}42$$

In the above equation, PEC_k is the purchased equipment cost, ϕ the total operating and maintenance cost factor (1.06), and t is the operating time of the system in one

year (7,446 hours). CRF (the capital recovery factor) is expressed by the following equation [85]:

$$CRF = \frac{i(1+i)^N}{(1-i)^N - 1} \quad 3\text{-}43$$

Here, i denotes the interest rate and n denotes the life of the system. In this thesis, in the thermoeconomic analysis, the interest rate is 10%, and the system life is 20 years [86].

Various parameters have been defined to make the thermoeconomic comparison. The first two parameters are the average cost per unit exergy of the fuel and product, determined as follows [87]:

$$c_{f,k} = \frac{\dot{C}_{f,k}}{\dot{E}x_f} \quad 3\text{-}44$$

$$c_{p,k} = \frac{\dot{C}_{p,k}}{\dot{E}x_p} \quad 3\text{-}45$$

The relative cost variance (r_k) is expressed in terms of the definition of the component's average cost per unit exergy of product and fuel [88]:

$$r_k = \frac{c_{p,k} - c_{f,k}}{c_{f,k}} \quad 3\text{-}46$$

The thermoeconomic factor (f_k) was defined as the ratio of the non-exergy-related cost to the contribution of the total cost increase, and the thermoeconomic factor is calculated with the following equation [88]:

$$f_k = \frac{\dot{Z}_k}{\dot{Z}_k + \dot{C}_{D,k}} \quad 3\text{-}47$$

$\dot{C}_{D,k}$ are the exergy destruction costs, and are calculated with the following equation:

$$\dot{C}_{D,k} = c_f \dot{E}x_{D,k} \quad 3\text{-}48$$

The cost balance and auxiliary equations of the components used in the system are shown in Table 4.5, and the initial investment cost functions for each component are shown in Table 4.6.

Finally, the total system cost is calculated with the following equation [89]:

$$\dot{C}_{system} = \sum \dot{z}_k + \sum \dot{C}_{D,k} \quad 3\text{-}49$$

The unit cost of the electricity produced by the system ($\dot{C}_{electricity}$) is another important parameter in cost analysis. This value expresses the total cost of the electricity and is calculated with the following equation [90]:

$$\dot{C}_{electricity} = \frac{\dot{C}_{system}}{\dot{W}_{NET}} \quad 3\text{-}50$$

Table 3. 5. Cost balance equations for system elements

Component	**Cost flow equations**	**Auxiliary equations**
HPT	$\dot{C}_1 + \dot{Z}_{HPT} = \dot{C}_2 + \dot{C}_{HPT}$	$c_1 = c_2$
IPT	$\dot{C}_3 + \dot{Z}_{IPT} = \dot{C}_5 + \dot{C}_{IPT}$	$c_3 = c_5, \quad c_3 = c_2$
LPT	$\dot{C}_6 + \dot{Z}_{LPT} = \dot{C}_8 + \dot{C}_{LPT}$	$c_6 = c_8, \quad c_6 = c_5$
Condenser	$\dot{C}_8 + \dot{C}_{15} + \dot{Z}_{Condenser} = \dot{C}_9 + \dot{C}_{16}$	$c_8 = c_9 \quad c_{15} = 0$
Pump1	$\dot{C}_9 + \dot{C}_{Pump1} + \dot{Z}_{pump1} = \dot{C}_{10}$	$c_{w.Pump1} = c_{w.LPT}$
OFWH1	$\dot{C}_7 + \dot{C}_{10} + \dot{Z}_{OFWH1} = \dot{C}_{11}$	$c_7 = c_5$
Pump2	$\dot{C}_{11} + \dot{C}_{Pump2} + \dot{Z}_{pump2} = \dot{C}_{12}$	$c_{w.Pump2} = c_{w.LPT}$
OFWH2	$\dot{C}_{12} + \dot{C}_4 + \dot{Z}_{OFWH2} = \dot{C}_{13}$	$c_4 = c_2$
Pump3	$\dot{C}_{13} + \dot{C}_{Pump3} + \dot{Z}_{pump3} = \dot{C}_{14}$	$c_{w.Pump3} = c_{w.LPT}$
Boiler	$\dot{C}_{19} + \dot{C}_{14} + \dot{Z}_{Boiler} = \dot{C}_1 + \dot{C}_{20}$	$c_{19} = c_{20}$
TES	$\dot{C}_{17} + \dot{C}_{21} + \dot{Z}_{TES} = \dot{C}_{19} + \dot{C}_{18}$	$c_{19} = c_{20}$
Pump4	$\dot{C}_{20} + \dot{C}_{Pump4} + \dot{Z}_{pump4} = \dot{C}_{21}$	$c_{w.Pump4} = c_{w.LPT}$
PTC	$\dot{C}_{18} + \dot{Z}_{PTC} = \dot{C}_{17}$	$c_{17} = c_{18}$

Table 3. 6. Initial investment cost functions of the sub-components of the system

Component	Investment cost	Reference source
HPT	$\dot{Z}_{HPT} = 6000\ \dot{W}_{HPT}^{0.7}$	[91,92]
IPT	$\dot{Z}_{IPT} = 6000\ \dot{W}_{IPT}^{0.7}$	[91,92]
LPT	$\dot{Z}_{LPT} = 6000\ \dot{W}_{LPT}^{0.7}$	[91,92]
Condenser	$\dot{Z}_{Condenser} = 1773\ \dot{m}_8$	[93]
Pump1	$\dot{Z}_{Pump1} = 2100\ \dot{W}_{pump1}{}^{0.26}\left(1-\eta_{Pump}/\eta_{Pump}\right)^{0,5}$	[62]
OFWH1	$\dot{Z}_{OFWH1} = 1773\ \dot{m}_{11}$	[94,95]
Pump2	$\dot{Z}_{Pump2} = 2100\ \dot{W}_{pump2}{}^{0.26}\left(1-\eta_{Pump}/\eta_{Pump}\right)^{0,5}$	[94]
OFWH2	$\dot{Z}_{OFWH2} = 1773\ \dot{m}_{13}$	[94,95]
Pump3	$\dot{Z}_{Pump3} = 2100\ \dot{W}_{pump3}{}^{0.26}\left(1-\eta_{Pump}/\eta_{Pump}\right)^{0,5}$	[94]
Boiler	$\dot{Z}_{Boiler} = \left(\frac{1}{1.12}\right) * 180 * \dot{Q}_{Boiler}$	[78]
TES	$\dot{Z}_{TES} = 1380 * v_{TES}$ and $v_{TES} = A_a/80$	[62,71,96]
Pump4	$\dot{Z}_{Pump4} = 2100\ \dot{W}_{pump4}{}^{0.26}\left(1-\eta_{Pump}/\eta_{Pump}\right)^{0,5}$	[94]
PTC	$\dot{Z}_{PTC} = 235 * A_a$	[97]

CHAPTER FOUR

EVALUATION AND DISCUSSION OF THE FINDINGS

Thermodynamic model equations in the analysis of the original concentrated solar power plant developed within the scope of this thesis have been used. The amount of product obtained from the system, energy and exergy efficiencies of the overall system, and exergy economic results were calculated. By changing important parameters, their effects on system performance and product costs are examined.
In the invested system, renewable energy is used to produce electricity. In order to ensure the continuity of the system, a thermal energy storage (TES) system is added to the solar energy cycle.

4.1. ENERGY AND EXERGY ANALYSIS RESULTS

Electricity is produced with three turbines in the invested system. These turbines are found in the Rankin cycle. The total electricity production obtained from the system is calculated as 39,895 kW. The amount of electricity produced by each turbine is given in Table 4.1. The highest power generation in the system was obtained from the LPT at 16,781 kW.

Table 4. 1. Electricity generation from turbines

Turbines	Power (kW)
HPT	13017
IPT	10094
LPT	16783
Total	39895

In order to obtain these products from the system, the amount of power drawn by the pumps is given in Table 4.2. The highest power consumption was calculated as 700.9 kW in Pump 3, and the total electricity consumed by the pumps was 897.66 kW.

Table 4. 2. Amount of power drawn by the pumps

Pumps	Power (kW)
Pump 1	36.06
Pump 1	160.7
Pump 3	700.9
Total	897.66

The mass flow rate, temperature, pressure, enthalpy, entropy and exergy values for each point in the developed system are calculated and shown in Table 4.3.

Table 4. 3. Thermodynamic properties for each point in the system

State	ṁ (kg/s)	P (bar)	T (°C)	h (kJ/kg)	S (kJ/kg. K)	x (-)	Ėx (MW)
1	42.44	150	545	3437	6.506	100	64.55
2	42.44	45	369.2	3130	6.592	100	50.46
3	33.95	45	369.2	3130	6.592	100	40.37
4	8.488	45	369.2	3130	6.592	100	10.09
5	33.95	10	201.9	2833	6.705	100	29.14
6	28.86	10	201.9	2833	6.705	100	24.77
7	5.093	10	201.9	2833	6.705	100	4.371
8	28.86	0.1235	50	2251	7.023	0.8573	5.282
9	28.86	0.1235	50	209.3	0.7038	0	0.1479
10	28.86	10	50.1	210.6	0.7046	-100	0.1773
11	33.95	10	143.3	603.9	1.773	-100	2.861
12	33.95	45	143.9	608.7	1.775	-100	2.999
13	42.44	45	255.6	1113	2.844	-100	11.77
14	42.44	150	259.1	1129	2.85	-100	12.4
15	1175		28.67	120.3	0.4183		0.2994
16	1175		40.67	170.4	0.5813		2.747
17	234.3	1.5	565	463.3	0.6863		61.12
18	234.3	1.5	287	40.44	0.07381		4.363
19	234.3	1.496	555	447.9	0.6676		58.79
20	234.3	1.491	280	29.98	0.05467		3.233
21	234.3	1.5	280	29.98	0.05467		3.233

The exergy analysis for each component of the concentrated solar power plant is shown in Figure 4.4. The current exergy values realized at all components of the system are seen. The results showed that the exergy value entering the system with

solar energy was 123.7 MW. The total product exergy obtained from the system is calculated as 39 MW. The table shows the highest exergy destruction occurs in the PTC at 66.93 MW. The exergy efficiency values of the components in the system are also shown in Figure 5.2. The PTC's lowest exergy efficiency was calculated as 45.9%, while the boiler and HPT achieved the highest exergy efficiency.

Table 4. 4. Exergy analysis for each component of the concentrated solar power plant

Component	$\dot{E}x_{input}$ **(MW)**	$\dot{E}x_{output}$ **(MW)**	$\dot{E}x_{destruction}$ **(MW)**	$\dot{E}x_{destruction}$ **(%)**	**Exergy efficiency (%)**
HPT	14.09	13.02	1.073	7	92.38
IPT	11.23	10.09	1.132	7.4	89.92
LPT	19.49	16.78	2.704	17.66	86.13
Condenser	5134	2.447	2.687	17.55	47.67
Pump 1	0.0361	0.0295	0.0066	0.043	81.75
OFWH 1	4.548	2.861	1.688	11.02	62.9
Pump 2	0.161	0.138	0.023	0.15	85.85
OFWH 2	13.09	1.77	1.317	8.6	89.94
Pump 3	0.7	0.623	0.078	0.51	88.91
Boiler	55.56	52.15	3.41	22.28	93.86
TES	56.75	55.56	1.192	7.8	97.9
PTC	123.7	56.75	66.93	-	45.89

Table 4.5 illustrates the total exergy input and exergy destruction for the system. The total exergy destruction for all components is approximately 82.255 MW, which accounts for approximately 66.34% of the system's total exergy inflow. Therefore, the available work net is 39 MW, at almost 31.45%. The remaining part of the exergy is released with the water flow through the condenser, at nearly 2.21%.

Table 4. 5. The model's energy input, output, and losses

Exergy	**Values (MW)**	**Percentage (%)**
Input	124	100%
Output (network)	39	31.45%
Exergy destruction	82.255	66.34%
Exergy losses	2.745	2.21%
Total	**124**	**100%**

Figure 4.1 presents the variation of exergy destruction for solar and other system components. The destruction of exergy is great when the temperature differences are higher. Thus, the highest rates for the destruction of exergy is calculated for the PTC, which has the largest temperature difference, at 81.2%.

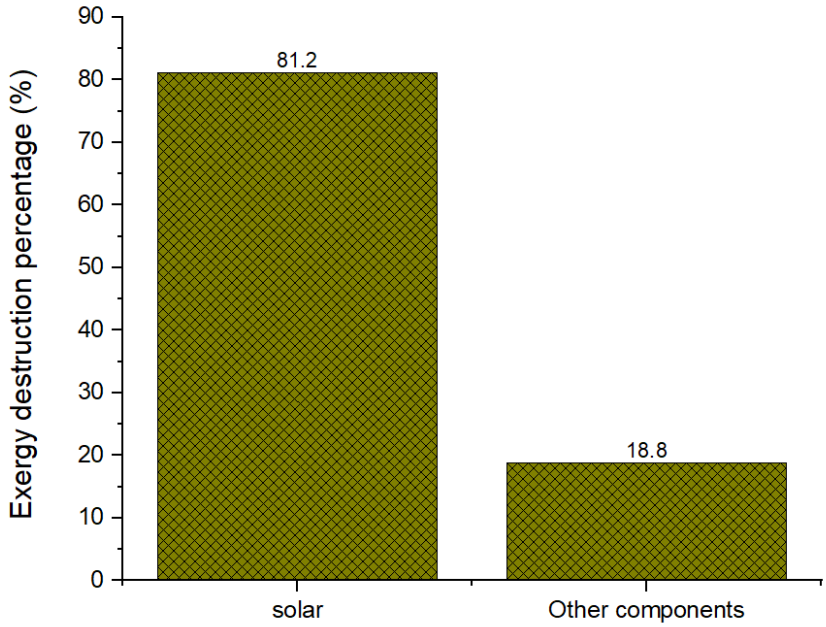

Figure 4. 1 The variation of exergy destruction for solar and another system component

The top components with the highest exergy destruction in the system, except for the PTC, are shown in Figure 4.2. The total exergy destruction in the system, except for the PTC, is 15.31 MW. Entropy production increases, and exergy destruction is calculated high in the boiler. The reason for the high exergy destruction in the

collector and boiler is the low solar collector efficiency and high entropy generation at high temperatures. The highest exergy destruction in the boiler was calculated as 3.41 MW. The second high exergy destruction was calculated as 2.7 for the LPT, as shown in Figure 4.2. The reason for the high exergy destruction in the turbine is the high entropy production. The lowest exergy destruction among the turbines was calculated as 1.073 kW in the HPT.

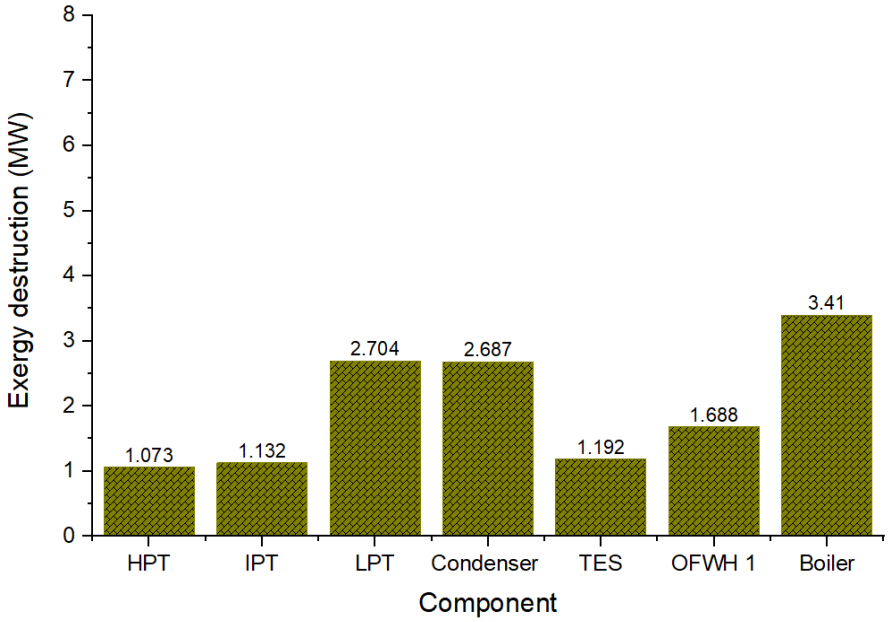

Figure 4. 2. Exergy destruction (MW) for the top components in the system

Figure 4.3 shows the components with the lowest exergy destruction in the system. The finding presents that the lowest exergy destruction values were found in the pumps. The lowest exergy destruction among the pumps was calculated as 0.0066 MW in Pump 1. The total amount of exergy destruction in the pumps was calculated as 0.7676 MW (approximately 0.93% of all exergy destruction). The reason for the low exergy destruction in the pumps is the low entropy production.

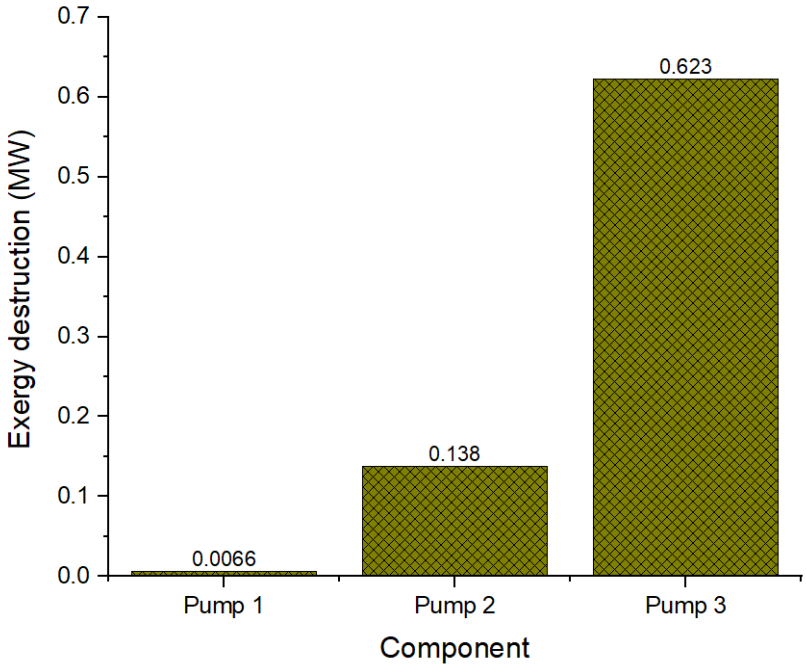

Figure 4. 3. Exergy destruction (MW) for the low components in the system

4.2. EXERGY ECONOMY ANALYSIS RESULTS

Exergy economics analysis, which is called thermoeconomics, is the examination of systems from both a thermodynamic and an economic point of view. In order to complete this analysis, thermodynamic properties were calculated in detail, and necessary analyses were made beforehand. Then, exergy currents, exergy loss, exergy efficiency, and exergy destruction were calculated for each flow point and each component in the system. The economic model was created with the cost equations. Product exergy and fuel exergy were determined for each component. Based on these data, the exergy economy analysis was completed. Table 4.6 presents cost rates and cost rates per unit of exergy of streams in the concentrated solar power plant. Furthermore, Table 4.7 shows exergy destruction, exergy efficiency, exergy destruction cost, and product cost for each component used in the system. The exergy-economic factor ($\boldsymbol{f_k}$) is shown along with the investment cost, which includes fuel cost, maintenance costs, and operating costs.

Table 4. 6. Cost rates and cost rates per unit of exergy of streams in the concentrated solar power plant

State	$\dot{C}$ ($/h)	c ($/GJ)
1	4010	17.26
2	3134	17.26
3	2508	17.26
4	626.9	17.26
5	1810	17.26
6	1539	17.26
7	271.5	17.26
8	328.1	17.26
9	9.186	17.26
10	12.67	19.85
11	311.7	30.26
12	326.1	30.21
13	987.3	23.3
14	1047	23.47
15	0	0
16	320.1	32.37
17	3035	13.79
18	216.7	13.79
19	2983	14.09
20	200.8	14.09
21	200.8	14.09

Exergy destruction in the system directly affects the investment cost. The total exergy destruction cost of the system was found to be 906.52 $/h. The highest exergy destruction cost is realized in the LPT at 167.94 $/h. The condenser is the second important component with high exergy destruction costs, at 166.07 $/h. The components with the lowest exergy destruction cost are pump1, pump2 and pump3.

Another important parameter that shows the relationship between investment and exergy destruction costs is the exergy-economic factor (f_k). If the f_k value is low, its efficiency should be increased by increasing the cost of the relevant component. In the calculations, the f_k value for the condenser and TES in the system was lower (< 14) compared to the other components. If the f_k value is high, it is necessary to

reduce the cost of the relevant component by considering the decrease in the efficiency value. In the system examined, the pump's f_k value was higher (> 93%).

The four components with the highest f_k value calculated in the system, excluding the pumps, are the HPT, IPT, boiler, and LPT. The f_k values for these system elements were calculated as 92.23%, 91.62%, 91.58%, and 86.72%, respectively. Considering the effect on efficiency values in these system elements, priority should be given to reducing costs compared to other system elements.

Table 4. 7. Exergy economy values are calculated for each component

Component	c_f **($/GJ)**	c_p **($/GJ)**	$\dot{C}_D$ **($/h)**	$\dot{Z}_K$ **($/h)**	$\dot{Z}_K + \dot{C}_D$ **($/h)**	r **(%)**	f **(%)**
HPT	17.26	20.19	66.633	70.867	137.5	17.01	93.23
IPT	17.26	20.82	70.294	59.306	129.6	20.67	91.62
LPT	17.26	21.44	167.94	84.66	252.6	24.23	86.72
Condenser	17.26	36.33	166.07	2.03	168.1	110.6	8.336
Pump 1	21.44	32.84	0.5075	0.7025	1.21	53.21	94.71
OFWH 1	17.36	30.26	105.42	27.48	132.9	74.36	77.16
Pump 2	21.44	29.06	1.755	2.03	3.785	35.54	93.75
OFWH 2	20.22	233	91.89	38.31	130.2	15.19	82.82
Pump 3	21.44	26.69	6.005	5.775	11.78	24.48	92.58
Boiler	13.91	15.78	170.8	143.4	314.2	13.44	91.58
TES	13.79	13.91	59.205	0.715	59.92	0.838	13.52
PTC	0	13.79	0	2818	2818	100	100
Total system	-	-	906.52	3253.28	4159.8	-	78.2

4.3. PARAMETRIC ANALYSIS

After obtaining the thermodynamic and economic results of the suggested system, the effects of the changes in the system parameters on the performance, cost, and amount of product obtained were investigated in detail.

The effects of parameters such as the amount of solar radiation, the pinch point, turbine isentropic efficiency, HPT extraction ratio, IPT extraction ratio, condenser

temperature, HPT pressure, IPT pressure, and LPT pressure on system performance and cost were investigated.

Figure 4.4 presents the output power of the studied plant in Aden. These values were computed for each month of the year. The findings show that the highest net output power was found in March and October. The cause of this behaviour is the high solar radiation in these months. The results present that the system produced 42.55 MW in March, whereas it produced 42.35 MW in October. The figure also presents that the lowest net output power was found in July.

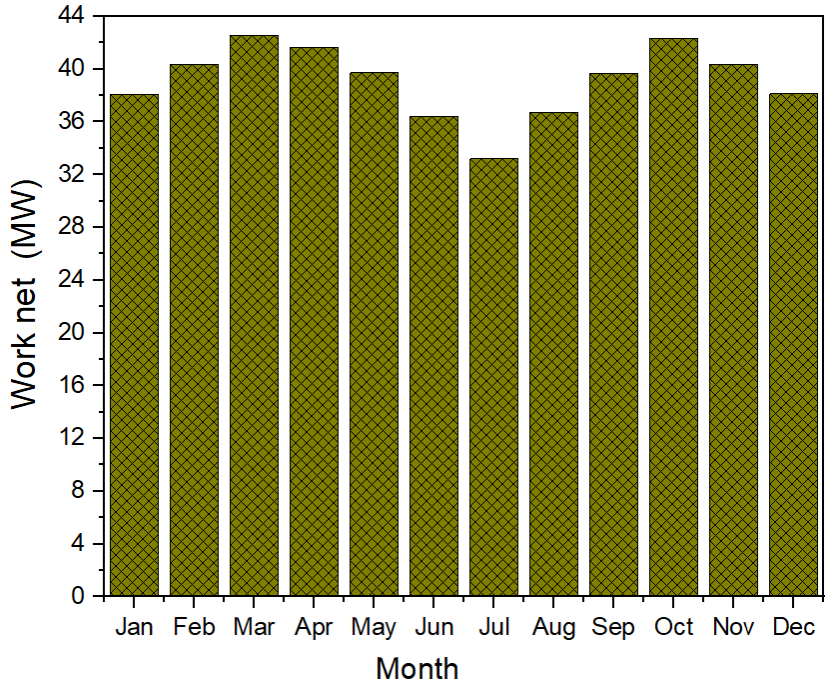

Figure 4. 4. The variation of the system's work net under each month

Figure 4.5 illustrates the value of the electrical cost for the studied plant for each month of the year. Although Figure 4.4 presents that the lowest net output power was in July, this month also has the maximum electrical cost. The results show the maximum electrical cost was 26.67 $/MWh in July, whereas the minimum was 23.36 $/MWh in October.

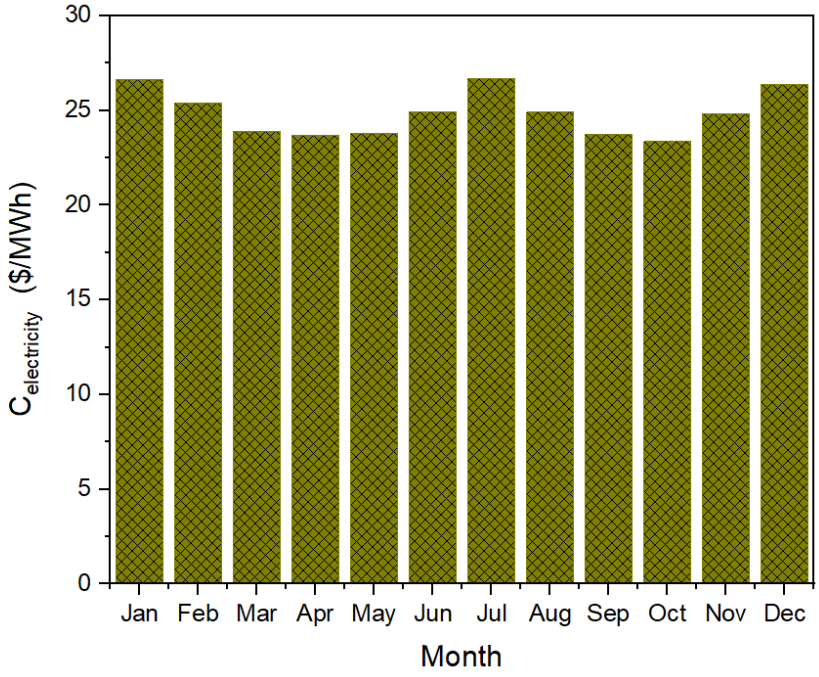

Figure 4. 5. The variation of the system's electricity cost rate for each month

The effect of the RC boiler's pinch point temperature difference on the performance and cost of the proposed system is illustrated in Figures 4.6 and 4.7. According to Table 4.8, increasing the RC boiler's pinch point temperature difference results in lower power output and overall efficiencies of the proposed system. The fundamental reason for this is that an increasing pinch point temperature causes a decrease in the enthalpy value at the inlet of each turbine; thus, the output power produced in the turbines decreases. On the other hand, with a decrement in outputs, the total cost rate first falls and then increases, as seen in Figure 4.6.

Table 4. 8. The performance and cost of the proposed system as a functionof the RC boiler's pinch point temperature difference

Pinch Point(°c)	$\dot{W}_{net}$ (MW)	$\dot{C}_{electricity}$ ($/MWh)	η_I (%)	η_{II} (%)
5	39.09	24.9	0.2995	0.3161
10	39	24.84	0.2988	0.3153
15	38.9	24.86	0.2981	0.3145
20	38.81	24.92	0.2973	0.3137
25	38.71	24.99	0.2966	0.313
30	38.62	25.07	0.2959	0.3122

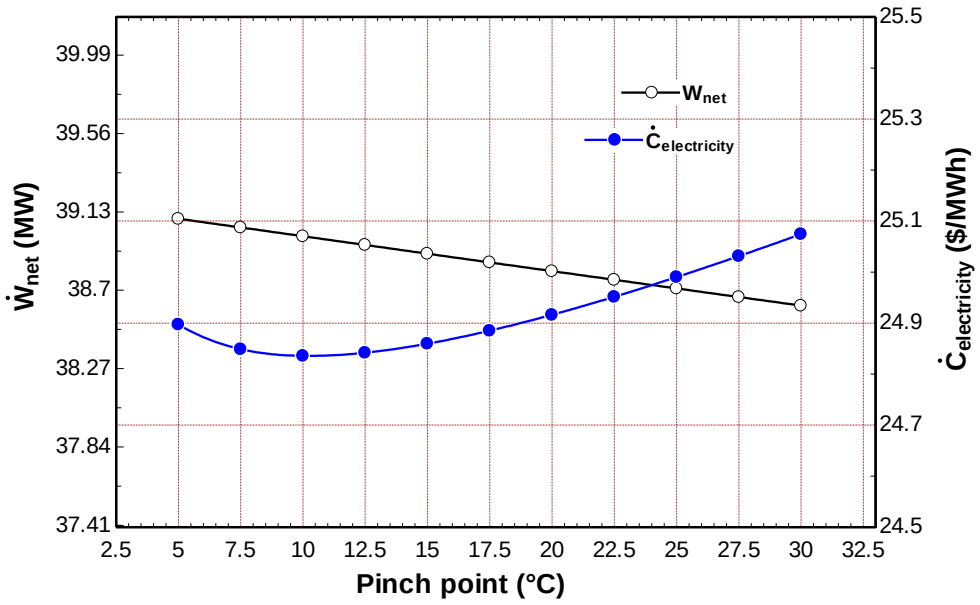

Figure 4. 6. Work net and electricity cost rate of the proposed system as a function of RC boiler's pinch point temperature difference

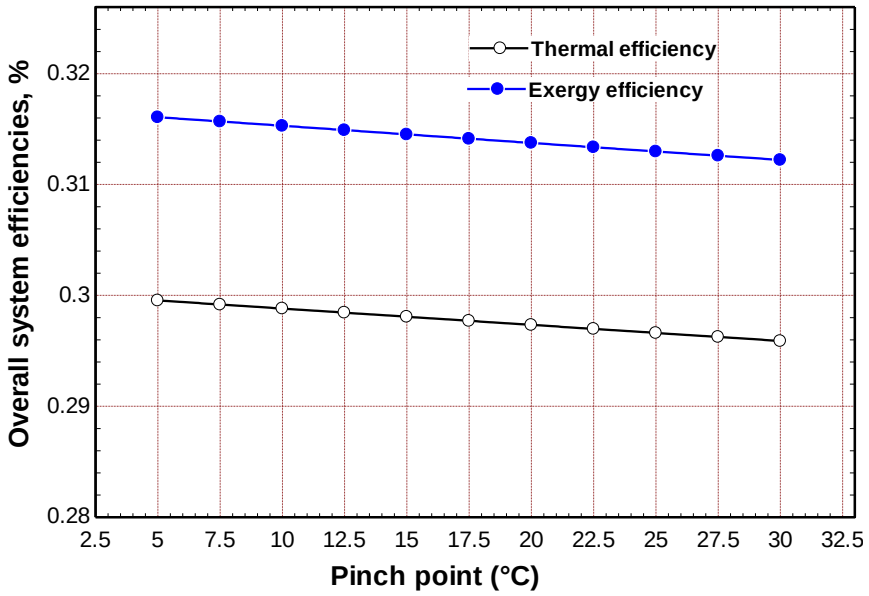

Figure 4. 7. Overall efficiencies of the proposed system as a function of RC boiler's pinch point temperature difference.

Figures 4.8 and 4.9 show the effect of the turbine isentropic efficiency on the proposed system's performance and cost. According to Table 4.9, increasing the η_T results in higher power output and overall efficiencies of the proposed system. The fundamental reason for this is that expanding the η_T turbine causes an increase in the thermal power converted to mechanical energy for each turbine, and the output power produced in the proposed system increases. In contrast, as shown in Figure 4.8, the total cost rate decreases as outputs increase.

Table 4. 9. The performance and cost of the proposed system as a function of the turbine isentropic efficiency

η_T (%)	$\dot{W}_{net}$ (MW)	$\dot{C}_{electricity}$ ($/MWh)	η_I (%)	η_{II} (%)
0.7	33.32	39.05	0.2553	0.2694
0.75	35.26	33.66	0.2702	0.2851
0.8	37.15	28.95	0.2847	0.3004
0.85	39	24.84	0.2988	0.3153
0.9	40.81	21.17	0.3127	0.3299
0.7	33.32	39.05	0.2553	0.2694

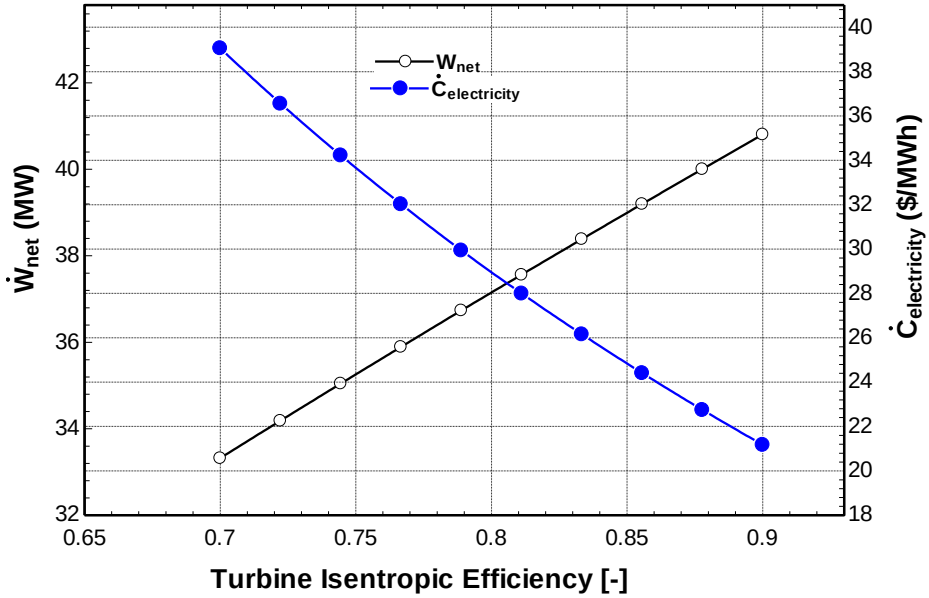

Figure 4. 8. Work net and electricity cost rate of the proposed system as a function of the turbine isentropic efficiency

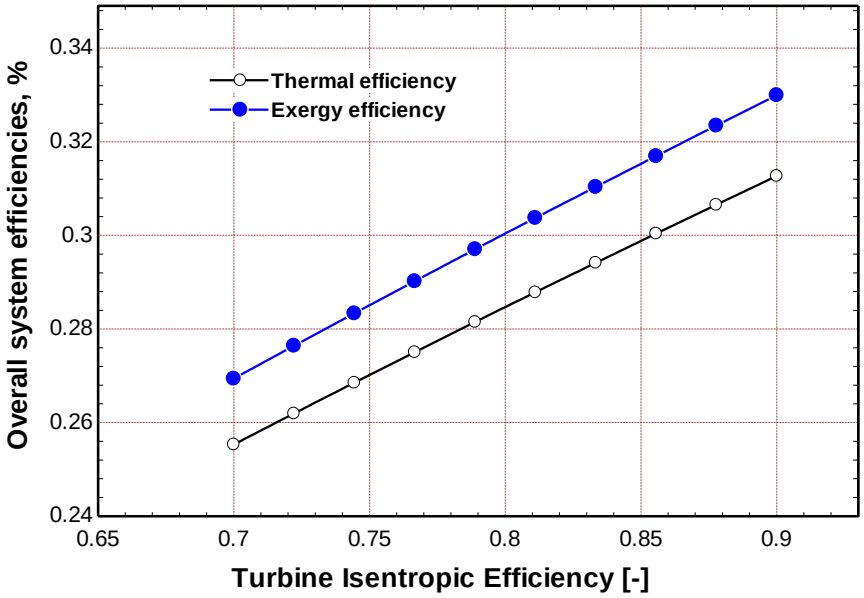

Figure 4. 9. Overall efficiencies of the proposed system as a function of turbine isentropic efficiency.

Figures 4.10 and 4.11 show the impact of steam extraction from the HPT (y_1) on the proposed system's performance and cost. Table 4.10 shows that the power output and overall efficiencies of the proposed system improve as the amount of steam extracted from the HPT increases. The main reason behind this is that increasing the quantity of steam extracted from the HPT causes a higher mass flow rate of steam,

and the enthalpy at the inlet of the boiler also increases; thus, the output power generated in the turbines increases. Figure 4.10 shows that the total cost rate increases as system outputs increase.

Table 4. 10. The performance and cost of the proposed system as a function of the HPT extraction ratio

y_1 (%)	$\dot{W}_{net}$ (MW)	$\dot{C}_{electricity}$ ($/MWh)	η_I (%)	η_{II} (%)
0.05	37.85	24.05	0.29	0.306
0.1	38.19	24.59	0.2927	0.3088
0.15	38.58	24.8	0.2956	0.3119
0.2	39	24.84	0.2988	0.3153

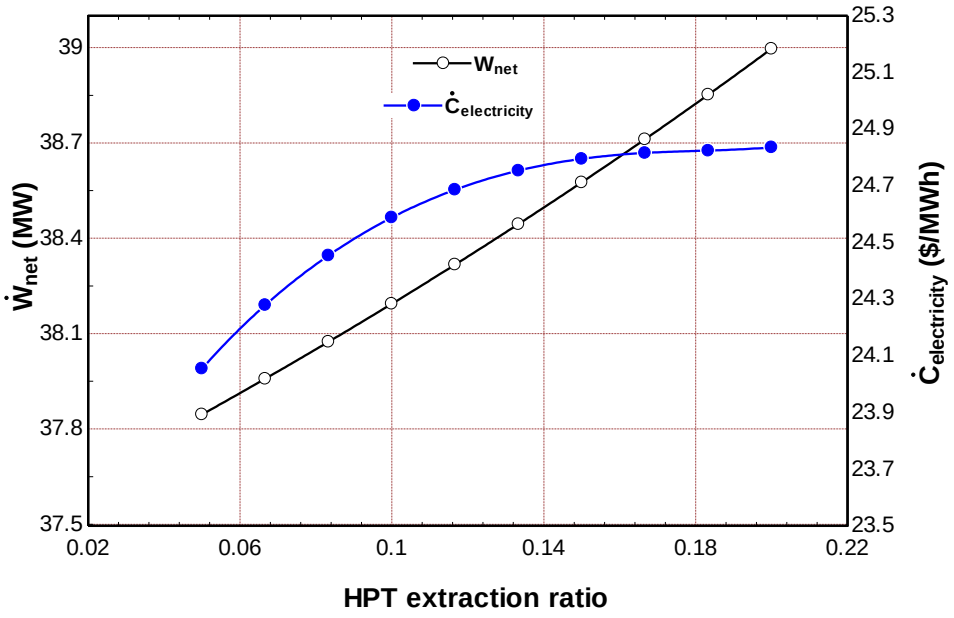

Figure 4. 10. Work net and electricity cost rate of the proposed system as a function of HPT extraction ratio

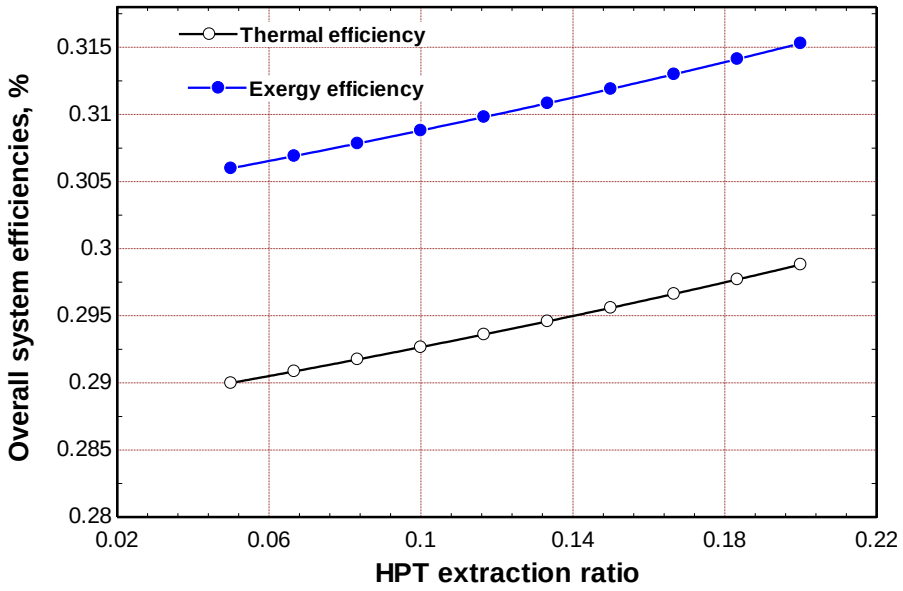

Figure 4. 11. Overall efficiencies of the proposed system as a function of HPT extraction ratio

The effect of steam extraction from the IPT (y_2) on the performance and cost of the proposed system is shown in Figures 4.12 and 4.13. As seen in Table 4.11, as the amount of steam extracted from the IPT rises, the proposed system's power output and overall efficiency increase. Figure 4.11 shows, as the amount of steam extracted from the IPT grows, the total cost rate initially drops and then rises. The lower total cost rate obtained at $y_1 = 0.18$ (approximately 24.41 \$/MWh).

Table 4. 11. The performance and cost of the proposed system as a function of the IPT extraction ratio

y_2 (%)	$\dot{W}_{net}$ (MW)	$\dot{C}_{electricity}$ (\$/MWh)	η_I (%)	η_{II} (%)
0.05	37.59	26.55	0.288	0.3039
0.1	38.26	25.81	0.2932	0.3094
0.15	39	24.84	0.2988	0.3153
0.2	39.74	24.9	0.3045	0.3213

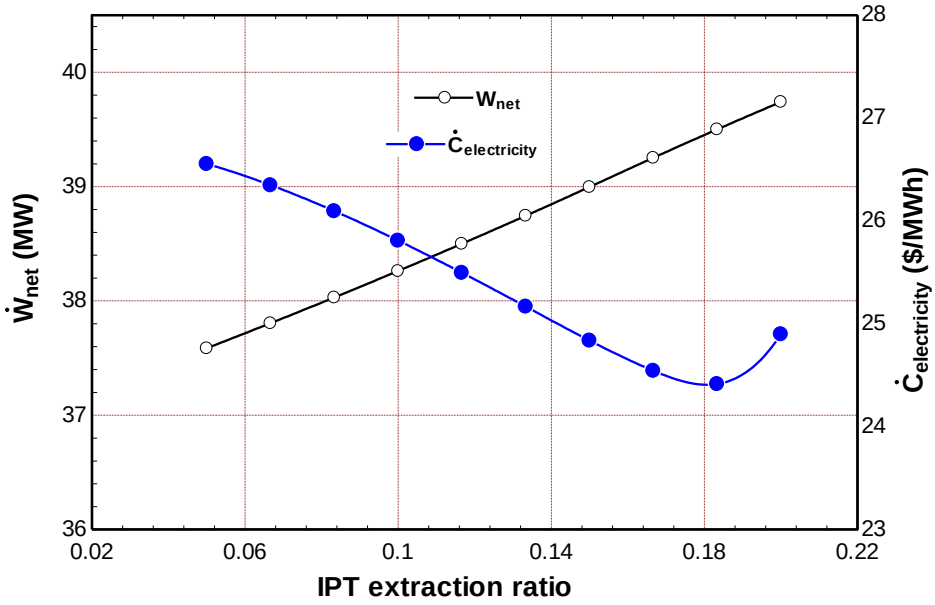

Figure 4. 12. Work net and electricity cost rate of the proposed system as a function of IPT extraction ratio

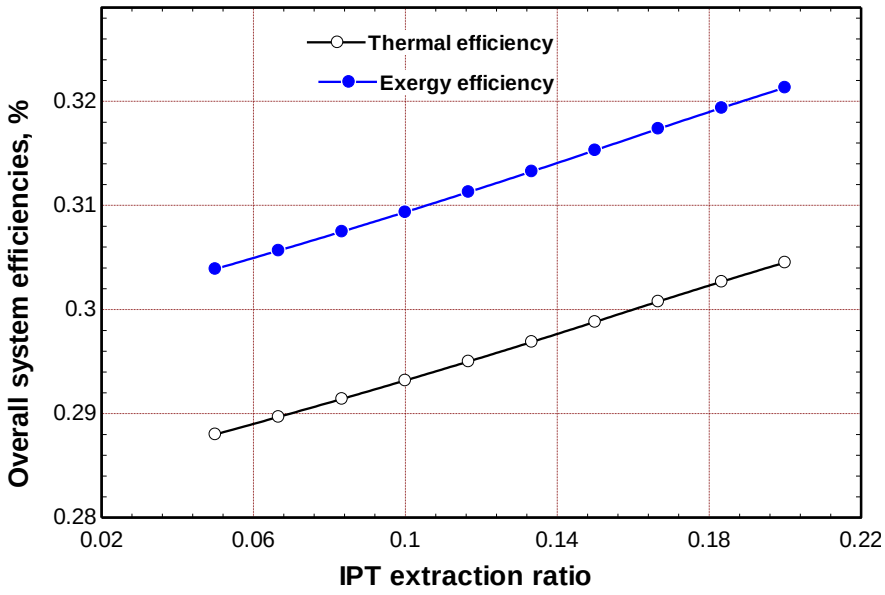

Figure 4. 13. Overall efficiencies of the proposed system as a function of IPT extraction ratio

Figures 4.14 and 4.15 describe the impact of the condenser temperature on the power output, overall efficiencies, and cost of the proposed system. As Table 4.12 indicates, increasing the condenser temperature reduces the power output, and total overall efficiencies of the power plant. The essential reason for this is that increasing the condenser temperature reduces the expansion process through the LPT and affects

the performance of the LPT. On the other hand, with the decrement in the power output, the total cost rate increases, as seen in Figure 4.14.

Table 4. 12. The performance and cost of the proposed system as a function of condenser temperature

$T_{condenser}$ (°C)	$\dot{W}_{net}$ (MW)	$\dot{C}_{electricity}$ ($/MWh)	η_I (%)	η_{II} (%)
35	40.5	21.84	0.3103	0.3275
40	40	22.81	0.3065	0.3234
45	39.5	23.81	0.3026	0.3193
50	39	24.84	0.2988	0.3153
55	38.5	25.89	0.295	0.3113
60	38	27	0.2912	0.3072
65	37.5	28.16	0.2874	0.3032
70	37	29.39	0.2835	0.2992
75	36.5	30.74	0.2797	0.2951
80	36	32.32	0.2758	0.291

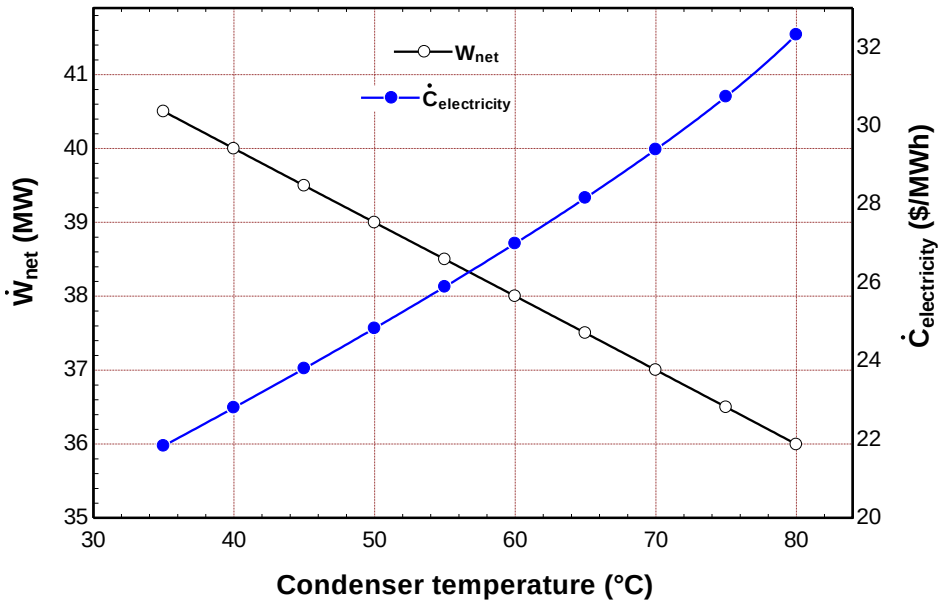

Figure 4. 14. Work net and electricity cost rate of the proposed system as a function of condenser temperature

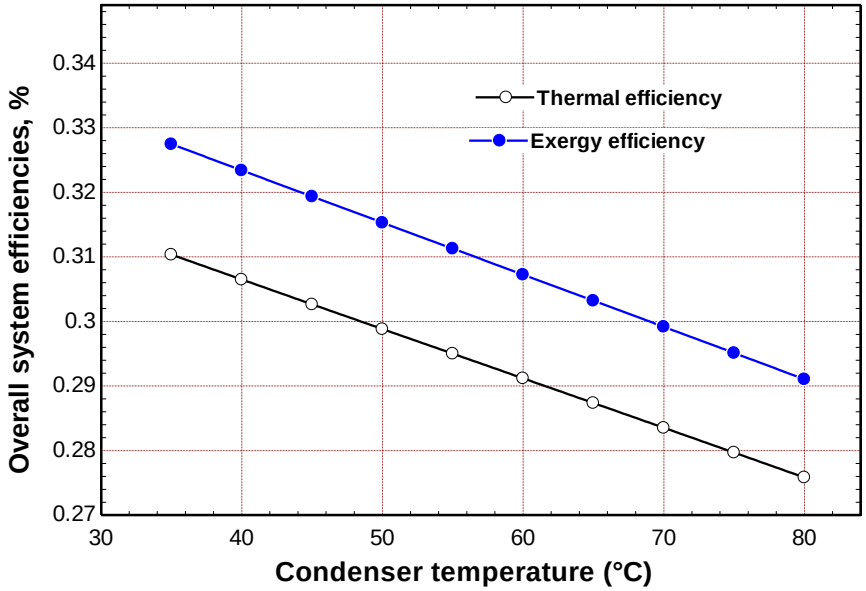

Figure 4. 15. Overall efficiencies of the proposed system as a function of condenser temperature

Table 4.13 presents the effect of the pressure at the beginning of the HPT (which is the input of the HPT) on the power output, efficiencies of the First and Second Laws, and total cost rate of the proposed system. For more clarity, Figure 4.16 and Figure 4.17 show the effect of the HPT's inlet pressure on the system's performance and cost. Obviously, increasing the HPT's inlet pressure also increases the $\dot{W}_{net}$, η_I, and η_{II} of the system. The virtual reason for this is that increasing HPT's inlet pressure causes an increase in the enthalpy value at the inlet of the HPT; thus, the output power produced in the HPT improves and affects both system efficiencies. Conversely, the total cost rate increases with an increment in outputs, as seen in Figure 4.16.

Table 4. 13. Overall efficiencies of the proposed system as a function of condenser temperature

P_{HPT} (bar)	$\dot{W}_{net}$ (MW)	$\dot{C}_{electricity}$ ($/MWh)	η_I (%)	η_{II} (%)
100	37.4	26.14	0.2866	0.3024
105	37.62	25.93	0.2882	0.3041
110	37.82	25.74	0.2898	0.3057
115	38	25.58	0.2912	0.3072
120	38.17	25.43	0.2925	0.3086
125	38.33	25.3	0.2937	0.3099
130	38.48	25.18	0.2949	0.3112
135	38.63	25.08	0.296	0.3123
140	38.76	24.98	0.297	0.3134
145	38.88	24.91	0.2979	0.3144
150	39	24.84	0.2988	0.3153
155	39.11	24.77	0.2996	0.3162
160	39.21	24.71	0.3004	0.317

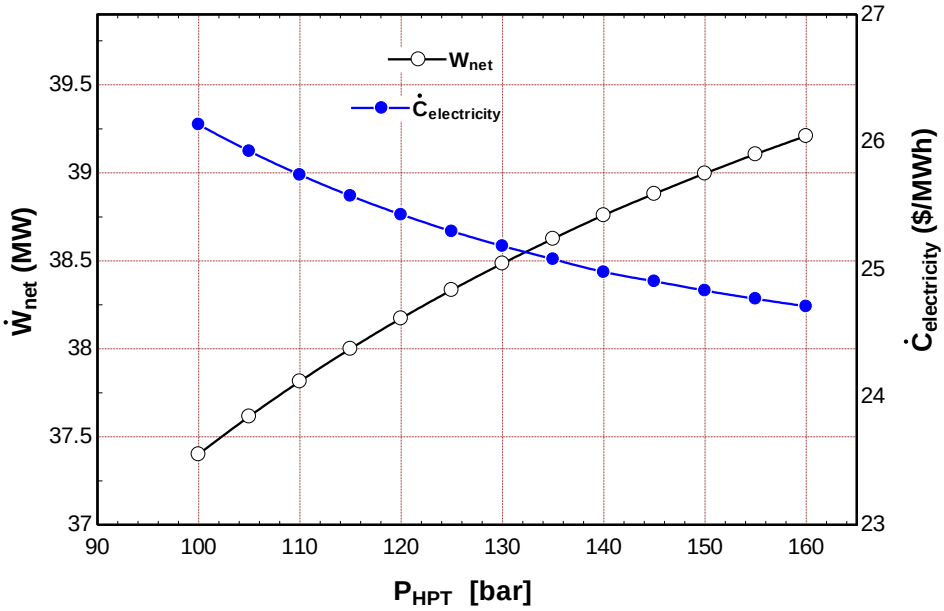

Figure 4. 16. Work net and electricity cost rate of the proposed system as a function of pressure at the beginning of HPT

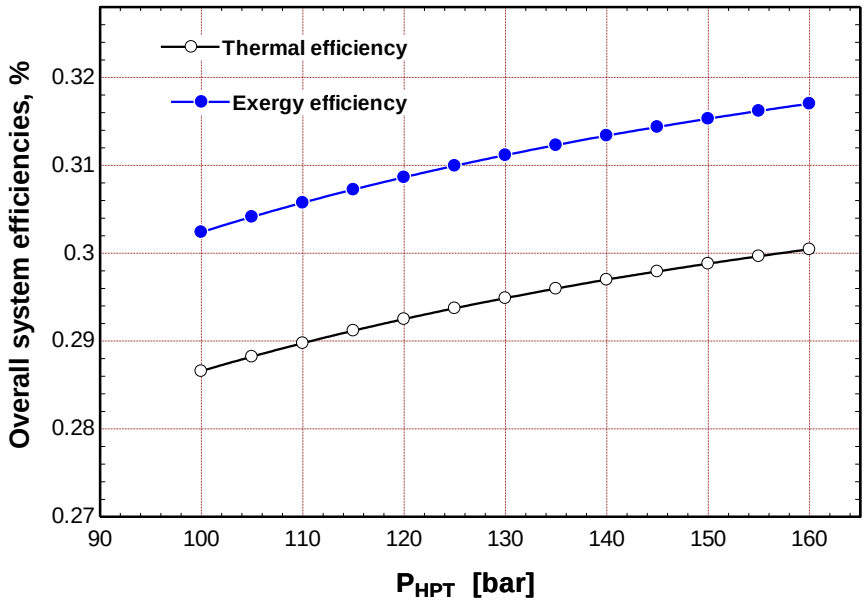

Figure 4. 17. Overall system efficiencies of the proposed system as a function of pressure at the beginning of HPT

Table 4.14 shows how the IPT's inlet pressure affects the system's power output, First- and Second-Law efficiencies, and overall cost rate. Figures 4.18 and 4.19 illustrate the impact of input pressure on IPT performance and cost, respectively. Clearly, increasing the IPT's inlet pressure also reduces the $\dot{W}_{net}$, η_I, and η_{II} , of the system. The essential explanation for this is that increasing the IPT's inlet pressure causes a large shortage in the work net of the HPT; thus, the output power produced by the system drops and reduces overall efficiencies. However, as shown in Figure 4.18, the system's overall cost rate rises as the IPT's inlet pressure increases.

Table 4. 14. The performance and cost of the proposed system as a function of pressure at the beginning of IPT

P_{IPT} (bar)	$\dot{W}_{net}$ (MW)	$\dot{C}_{electricity}$ ($/MWh)	η_I (%)	η_{II} (%)
20	39.53	23.09	0.3029	0.3196
25	39.46	23.36	0.3024	0.319
30	39.36	23.69	0.3016	0.3183
35	39.25	24.06	0.3007	0.3173
40	39.12	24.44	0.2998	0.3163
45	39	24.84	0.2988	0.3153
50	38.87	25.21	0.2979	0.3143
55	38.76	25.57	0.297	0.3134
60	38.64	25.9	0.2961	0.3124
65	38.54	26.22	0.2953	0.3116

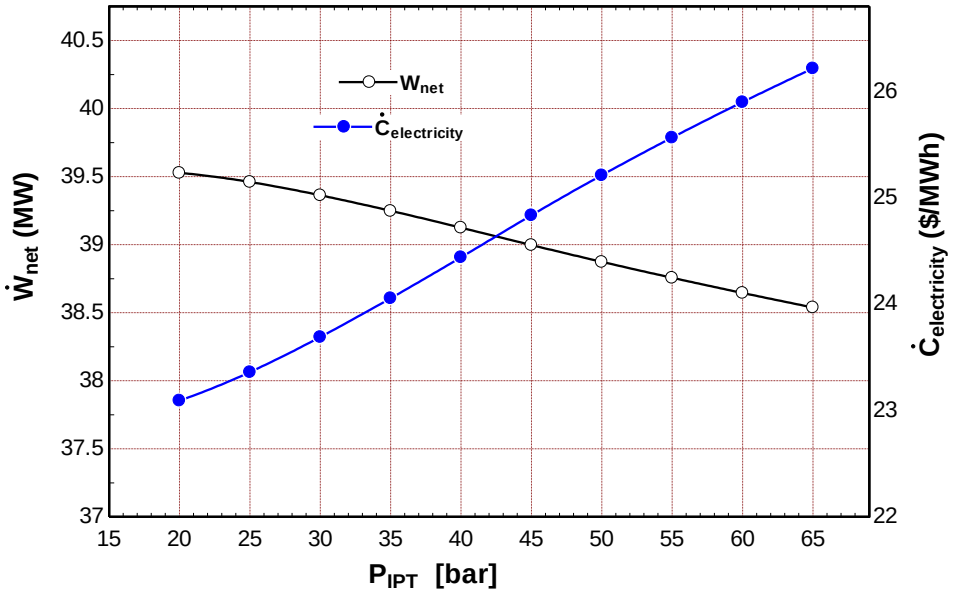

Figure 4. 18. Work net and electricity cost rate of the proposed system as a function of pressure at the beginning of IPT

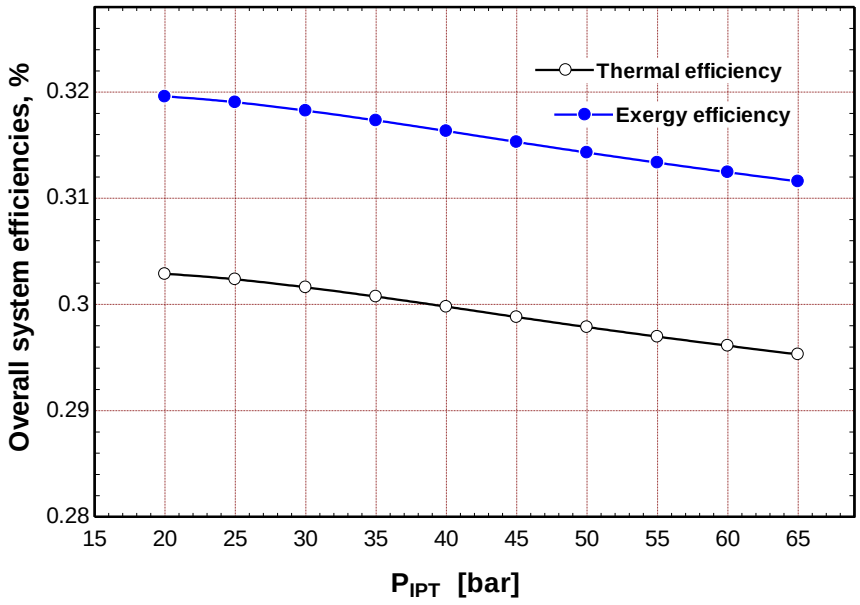

Figure 4. 19. Overall system efficiencies of the proposed system as a function of pressure at the beginning of IPT

Figures 4.20 and 4.21 show the efficiency impact of the LPT's inlet pressure on the proposed system's power output, overall efficiencies, and cost. As Table 4.15 shows, increasing the LPT's inlet pressure diminishes the power output and total overall efficiencies of the proposed system. Figure 4.20 shows that as LPT's inlet pressure increases, the work net of the IPT decreases, leading to lower system output power and worse overall efficiencies. However, as shown in Figure 4.21, the overall cost rate of the system increases as the LPT's inlet pressure rises.

Table 4. 15. The performance and cost of the proposed system as a function of pressure at the beginning of LPT

P_{LPT} (bar)	$\dot{W}_{net}$ (MW)	$\dot{C}_{electricity}$ ($/MWh)	η_I (%)	η_{II} (%)
10	39	24.84	0.2988	0.3153
10.5	38.97	24.91	0.2986	0.3151
11	38.94	24.98	0.2984	0.3149
11.5	38.92	25.06	0.2982	0.3147
12	38.89	25.13	0.298	0.3145
12.5	38.87	25.19	0.2978	0.3143
13	38.84	25.26	0.2976	0.3141
13.5	38.82	25.32	0.2975	0.3139
14	38.8	25.39	0.2973	0.3137
14.5	38.77	25.45	0.2971	0.3135

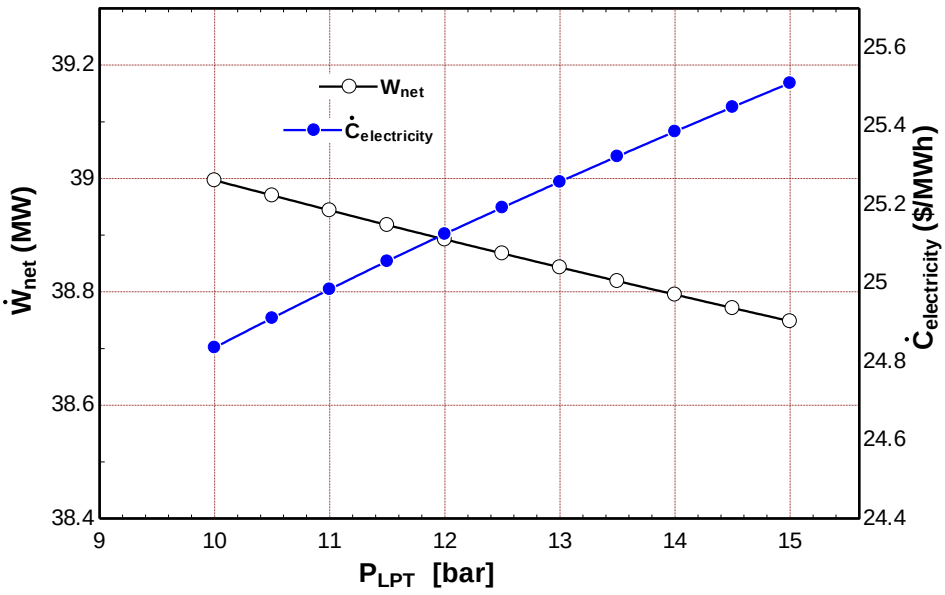

Figure 4. 20. Work net and electricity cost rate of the proposed system as a function of pressure at the beginning of LPT

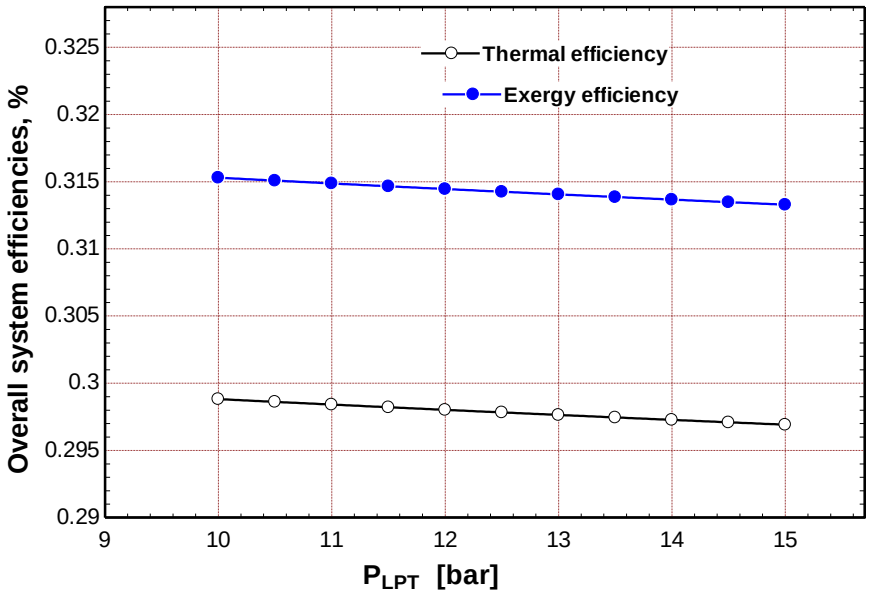

Figure 4. 21. Overall system efficiencies of the proposed system as a function of pressure at the beginning of LPT

CHAPTER FIVE

CONCLUSION AND FUTURE WORK

This study investigates the thermodynamic and exergoeconomic analyses of the performance of parabolic trough solar collectors integrated with thermal energy storage and the Rankine power cycle. Furthermore, a thermoeconomic analysis was performed for all components separately in the proposed system. The thermodynamic and exergoeconomic analysis results for the proposed system are as follows:

- The highest net output power was found in March, and the lowest net output power was found in July. These values were 42.55 MW and 33.2 MW, respectively.
- The lowest net output power occurred in July, with the maximum electrical cost. The system's electricity cost rate was 26.67 $/MWh during this month.
- The highest exergy destruction cost is realized in LPT as 167.94 $/h, and the condenser is the second important component with high exergy destruction costs, at 166.07 $/h.
- A decrease in the boiler's pinch point leads to a reduction in the power output and a decrease in the overall efficiencies of the system. The decrease in the power outputs leads to falls in the total cost rate first and then increases. The optimum value for the total cost rate was obtained at 10℃.
- By increasing the turbine's isentropic efficiency, the power output increases and leads to higher energy and exergy efficiencies and a reduction in the total cost rate of the system.
- The power output and overall efficiencies of the proposed system improve as the amount of steam extracted from the HPT and IPT increases.
- By increasing the steam extracted from the IPT, the total cost rate initially drops and then rises. The lower total cost rate is obtained at $y_1 = 0.18$ (approximately 24.41 $/MWh).

- By increasing the condenser temperature, the power output decreases, leading to lower energy and exergy efficiencies and an increment in the total cost rate of the system.
- Increasing the inlet pressure at IPT and LPT decreases the proposed system's power output and overall efficiencies and increases the cost rate.
- Increasing the inlet pressure at HPT improves the proposed system's power output and overall efficiencies and reduces the cost rate.

The results obtained from this study are both a thermodynamic and exergoeconomic guide for energy production from renewable energy sources in Yemen, which suffers from a severe shortage of electricity. The proposed system can be developed in future studies with other renewable sources or by using a transient analysis for thermal energy storage to generate electricity at night or when solar energy is unavailable.

REFERENCES

1. Jiang, Y., Hajivand, M., Sadeghi, H., Gerdroodbary, M. B., and Li, Z., "Influence of trapezoidal lobe strut on fuel mixing and combustion in supersonic combustion chamber", Aerospace Science And Technology, 116: 106841 (2021).

2. Bo, J., Vellore, J., and Holm-nielsen, B., "Large Scale Renewable Energy Integration : Energy Integration : and Solutions", Energies, 12, (10): 1–17 (2019).
3. Hamzah, A. H., Akroot, A., and Jaber, J. A., "Analytical Investigation of Biodiesel Mixed Levels and Operation Factors' Effects on Engine Performance by RCM", International Journal Of Design And Nature And Ecodynamics, 17 (6): 863–873 (2022).

4. Shawky, M. and Moursi, E., "Wind speed and solar irradiance forecasting techniques for enhanced renewable energy integration with the grid : a review", .

5. Siegel, N. P., "Thermal energy storage for solar power production", Energy And Environment, 1 (October): 119–131 (2012).

6. Mostafavi, S. S., Shoraka, Y., Nithyanandam, K., and Taylor, R. A., "Shell-and-tube or packed bed thermal energy storage systems integrated with a concentrated solar power : A techno-economic comparison of sensible and latent heat systems", Applied Energy, 238 (November 2017): 887–910 (2019).

7. Mostafavi, S. S., Saffar-avval, M., Behboodi, S., and Mansoori, Z., "Hourly energy analysis and feasibility study of employing a thermocline TES system for an integrated CHP and DH network", Energy Conversion And Management, 68: 281–292 (2013).

8. Romero, M., "Solar thermal CSP technology", Energ And Environment, 3 (February 2014): (2020).

9. Dawood, T. A., Raphael, R., Barwari, I., and Akroot, A., "Solar Energy and Factors Affecting the Efficiency and Performance of Panels in Erbil / Kurdistan", 41 (2): 304–312 (2023).

10. Temraz, A., Rashad, A., Elweteedy, A., and Elshazly, K., "Thermal Analysis of the Iscc Power Plant in Kuraymat, Egypt", The International Conference On Applied Mechanics And Mechanical Engineering, 18 (18): 1–15 (2018).

11. Zhang, H. L., Baeyens, J., Degrève, J., and Cacères, G., "Concentrated solar power plants: Review and design methodology", Renewable And Sustainable Energy Reviews, 22: 466–481 (2013).

12. Olfian, H., Soheil, S., Ajarostaghi, M., and Ebrahimnataj, M., "Development on evacuated tube solar collectors : A review of the last decade results of using nanofluids", Solar Energy, 211 (July): 265–282 (2020).

13. Kim, Y., Han, G., and Seo, T., "An evaluation on thermal performance of CPC solar collector ☆", 35: 446–457 (2008).

14. Khudhur, J., Akroot, A., and Al-samari, A., "Experimental Investigation of Direct Solar Photovoltaics that Drives Absorption Refrigeration System", 1 (1): 116–135 (2023).

15. Aggarwal, S., Kumar, R., Lee, D., Kumar, S., and Singh, T., "A comprehensive review of techniques for increasing the efficiency of evacuated tube solar collectors", Heliyon, 9 (4): e15185 (2023).

16. Evangelisti, L., Vollaro, R. D. L., and Asdrubali, F., "Latest advances on solar thermal collectors : A comprehensive review", Renewable And Sustainable Energy Reviews, 114 (August): 109318 (2019).

17. Dobriyal, R., Negi, P., Sengar, N., and Singh, D. B., "A brief review on solar flat plate collector by incorporating the effect of nanofluid", Materials Today: Proceedings, 21: 1653–1658 (2020).

18. Ram, S., Yadav, S. K., and Kumar, A., "Recent advancement of nanofluids in solar concentrating collectors : A brief review", Materials Today: Proceedings, 72: 2032–2038 (2023).

19. Assaf, Y. H., Akroot, A., Abdul Wahhab, H. A., Talal, W., Bdaiwi, M., and Nawaf, M. Y., "Impact of Nano Additives in Heat Exchangers with Twisted Tapes and Rings to Increase Efficiency: A Review", Sustainability (Switzerland), 15 (10): (2023).

20. Ebrazeh, S. and Sheikholeslami, M., "Applications of nanomaterial for parabolic trough collector", Powder Technology, 375: 472–492 (2020).

21. Naveenkumar, R., Ravichandran, M., Stalin, B., Ghosh, A., Karthick, A., Kumar, S. P., and Kumar, S. K., "Comprehensive review on various parameters that influence the performance of parabolic trough collector", 22310–22333 (2021).

22. Riahi, S., Jovet, Y., Saman, W. Y., Belusko, M., and Bruno, F., "Sensible and latent heat energy storage systems for concentrated solar power plants , exergy efficiency comparison", Solar Energy, 180 (August 2018): 104–115 (2019).

23. Naveenkumar, R., Ravichandran, M., Mohanavel, V., Karthick, A., Kiran, S., Shanmugavelan, K., and Kumar, P., "Review on Phase Change Materials for Solar Energy Storage Applications", Environmental Science and Pollution Research, Springer Berlin Heidelberg, 9491–9532 (2022).
24. Colella, F., Sciacovelli, A., and Verda, V., "Numerical analysis of a medium scale latent energy storage unit for district heating systems", Energy, 45 (1): 397–406 (2012).

25. Dolado, P., Gil, A., Medrano, M., Martorell, I., La, A., and Cabeza, L. F., "State of the art on high temperature thermal energy storage for power generation . Part 1 — Concepts , materials and modellization", 14: 31–55 (2010).

26. Olivkar, P. R., Katekar, V. P., Deshmukh, S. S., and Palatkar, S. V, "Effect of sensible heat storage materials on the thermal performance of solar air heaters : State-of-the-art review", Renewable And Sustainable Energy Reviews, 157 (January): 112085 (2022).

27. Hameer, S. and Niekerk, J. L. Van, "A review of large-scale electrical energy storage", Int J Energy Res, (February): 1179–1195 (2015).

28. Opolot, M., Zhao, C., Liu, M., Mancin, S., and Bruno, F., "A review of high temperature ($\geq 500 \circ C$) latent heat thermal energy storage", Renewable And Sustainable Energy Reviews, 160 (March): (2022).

29. Li, Z., "Heat transfer enhancement of latent heat thermal energy storage in solar heating system : A state-of-the-art review", Journal Of Energy Storage, 46 (November 2021): (2022).

30. Sharma, A., Tyagi, V. V, Chen, C. R., and Buddhi, D., "Review on thermal energy storage with phase change materials and applications", 13: 318–345 (2009).

31. Khudhair, A. M. and Farid, M. M., "A review on energy conservation in building applications with thermal storage by latent heat using phase change materials", 45: 263–275 (2004).

32. Wu, S., Zhou, C., Doroodchi, E., Nellore, R., and Moghtaderi, B., "A review on high-temperature thermochemical energy storage based on metal oxides redox cycle", Energy Conversion And Management, 168 (March): 421–453 (2018).

33. Felderhoff, M., Urbanczyk, R., and Peil, S., "Thermochemical Heat Storage for High Temperature Applications – A Review", Green, 3 (2): 113–123 (2013).

34. Liu, M., Riahi, S., Jacob, R., Belusko, M., and Bruno, F., "Design of sensible and latent heat thermal energy storage systems for concentrated solar power plants: Thermal performance analysis", Renewable Energy, 151: 1286–1297 (2020).

35. Mukherjee, S. S., Meshram, H. A., Rakshit, D., and Saha, B. B., "A comparative study of sensible energy storage and hydrogen energy storage apropos to a concentrated solar thermal power plant", Journal Of Energy Storage, 61 (February): 106629 (2023).
36. Alqahtani, T., "Performance evaluation of a solar thermal storage system proposed for concentrated solar power plants", Applied Thermal Engineering, 229 (April): 120665 (2023).

37. Bouziane, H. and Benhamou, B., "Assessment of the impact of thermal energy storage operation strategy on parabolic trough solar power plant performance", Renewable Energy, 202 (November 2022): 713–720 (2023).

38. Qin, J., Long, X., Zhang, Q., Hu, E., Zhang, H., Duan, J., and Zhou, Y., "Impact of thermal energy storage system on the Solar Aided Power Generation plant with diverse structure and extraction steam operation strategy", Applied Thermal Engineering, 221 (November 2022): 119801 (2023).

39. Luo, Y., Du, X., Yang, L., Xu, C., and Amjad, M., "Impacts of solar multiple on the performance of direct steam generation solar power tower plant with integrated thermal storage", Frontiers In Energy, 11 (4): 461–471 (2017).

40. Talal, W. . and Akroot, A., "Exergoeconomic Analysis of an Integrated Solar Combined Cycle in the Al-Qayara Power Plant in Iraq", Processes, 11, 656.: (2023).

41. Jiang, Y., Duan, L., Yang, M., Tong, Y., and Pang, L., "Performance analysis of tower solar aided coal-fired power plant with thermal energy storage", Applied Thermal Engineering, 206 (July 2021): 118101 (2022).

42. Liu, M., Jacob, R., Belusko, M., Riahi, S., and Bruno, F., "Techno-economic analysis on the design of sensible and latent heat thermal energy storage systems for concentrated solar power plants", Renewable Energy, 178: 443–455 (2021).

43. Khamlich, I., Zeng, K., Flamant, G., Baeyens, J., Zou, C., Li, J., Yang, X., He, X., Liu, Q., Yang, H., Yang, Q., and Chen, H., "Technical and economic assessment of thermal energy storage in concentrated solar power plants within a spot electricity market", Renewable And Sustainable Energy Reviews, 139 (July 2019): 110583 (2021).

44. Monjurul Ehsan, M., Guan, Z., Gurgenci, H., and Klimenko, A., "Novel design measures for optimizing the yearlong performance of a concentrating solar thermal power plant using thermal storage and a dry-cooled supercritical CO2 power block", Energy Conversion And Management, 216 (May): 112980 (2020).

45. Chen, R., Rao, Z., Liao, S., Liu, G., and Li, D., "Analysis and optimization the size of heliostat field and thermal energy storage for solar tower power plants", Energy Procedia, 158: 712–717 (2019).

46. d’Entremont, A., Corgnale, C., Hardy, B., and Zidan, R., "Simulation of high temperature thermal energy storage system based on coupled metal hydrides for solar driven steam power plants", International Journal Of Hydrogen Energy, 43 (2): 817–830 (2018).
47. Prieto, C., Rodríguez, A., Patiño, D., and Cabeza, L. F., "Thermal energy storage evaluation in direct steam generation solar plants", Solar Energy, 159 (November 2017): 501–509 (2018).

48. Ciani Bassetti, M., Consoli, D., Manente, G., and Lazzaretto, A., "Design and off-design models of a hybrid geothermal-solar power plant enhanced by a thermal storage", Renewable Energy, 128: 460–472 (2018).

49. Peiró, G., Prieto, C., Gasia, J., Jové, A., Miró, L., and Cabeza, L. F., "Two-tank molten salts thermal energy storage system for solar power plants at pilot plant scale: Lessons learnt and recommendations for its design, start-up and operation", Renewable Energy, 121: 236–248 (2018).

50. Pelay, U., Luo, L., Fan, Y., Stitou, D., and Rood, M., "Thermal energy storage systems for concentrated solar power plants", Renewable And Sustainable Energy Reviews, 79 (March 2016): 82–100 (2017).

51. Andika, R., Kim, Y., Yoon, S. H., Kim, D. H., Choi, J. S., and Lee, M., "Techno-economic assessment of technological improvements in thermal energy storage of concentrated solar power", Solar Energy, 157 (August): 552–558 (2017).

52. Adibhatla, S. and Kaushik, S. C., "Energy, exergy, economic and environmental (4E) analyses of a conceptual solar aided coal fired 500 MWe thermal power plant with thermal energy storage option", Sustainable Energy Technologies And Assessments, 21: 89–99 (2017).

53. Pizzolato, A., Donato, F., Verda, V., Santarelli, M., and Sciacovelli, A., "CSP plants with thermocline thermal energy storage and integrated steam generator – Techno-economic modeling and design optimization", Energy, 139: 231–246 (2017).

54. Grange, B., Dalet, C., Falcoz, Q., Ferrière, A., and Flamant, G., "Impact of thermal energy storage integration on the performance of a hybrid solar gas-turbine power plant", Applied Thermal Engineering, 105: 266–275 (2016).

55. Rodríguez, J. M., Sánchez, D., Martínez, G. S., Bennouna, E. G., and Ikken, B., "Techno-economic assessment of thermal energy storage solutions for a 1 MWe CSP-ORC power plant", Solar Energy, 140: 206–218 (2016).

56. Chacartegui, R., Vigna, L., Becerra, J. A., and Verda, V., "Analysis of two heat storage integrations for an Organic Rankine Cycle Parabolic trough solar power plant", Energy Conversion And Management, 125: 353–367 (2016).

57. Casati, E., Casella, F., and Colonna, P., "Design of CSP plants with optimally operated thermal storage", Solar Energy, 116: 371–387 (2015).

58. Tehrani, S. S. M. and Taylor, R. A., "Off-design simulation and performance of molten salt cavity receivers in solar tower plants under realistic operational modes and control strategies", Applied Energy, 179: 698–715 (2016).

59. MORAN, M. J. and SHAPIRO, HOWARD N.BOETTNER, D. D. M. B. B., "Fundamentals of Engineering Thermodynamics", WILEY, 14–61 (2020).

60. Cengel, Y. A. and Boles, M. A., "Thermodynamics: An Engineering Approach 8th Edition", McGraw-Hill, (2015).

61. Kareem, A. F., Akroot, A., Wahhab, H. A. A., Talal, W., Ghazal, R. M., and Alfaris, A., "Exergo – Economic and Parametric Analysis of Waste Heat Recovery from Taji Gas Turbines Power Plant Using Rankine Cycle and Organic Rankine Cycle", (2023).

62. Aghaziarati, Z. and Aghdam, A. H., "Thermoeconomic analysis of a novel combined cooling, heating and power system based on solar organic Rankine cycle and cascade refrigeration cycle", Renewable Energy, 164: 1267–1283 (2021).

63. Zarza, E., Rojas, M. E., González, L., Caballero, J. M., and Rueda, F., "INDITEP: The first pre-commercial DSG solar power plant", Solar Energy, 80 (10): 1270–1276 (2006).

64. Yüksel, Y. E., "Thermodynamic assessment of modified Organic Rankine Cycle integrated with parabolic trough collector for hydrogen production", International Journal Of Hydrogen Energy, 43 (11): 5832–5841 (2018).
65. Shahin, M. S., Orhan, M. F., and Uygul, F., .

66. Ozlu, S. and Dincer, I., "Performance assessment of a new solar energy-based multigeneration system", Energy, 112: 164–178 (2016).

67. Alperen, M. A., Kayabaşi, E., and Kurt, H., "Detailed comparison of the methods used in the heat transfer coefficient and pressure loss calculation of shell side of shell and tube heat exchangers with the experimental results", Energy Sources, Part A: Recovery, Utilization, And Environmental Effects, 45 (2): (2023).

68. Al-Sulaiman, F. A., Hamdullahpur, F., and Dincer, I., "Performance assessment of a novel system using parabolic trough solar collectors for combined cooling, heating, and power production", Renewable Energy, 48: 161–172 (2012).

69. Toghyani, S., Baniasadi, E., and Afshari, E., "Thermodynamic analysis and optimization of an integrated Rankine power cycle and nano-fluid based parabolic trough solar collector", Energy Conversion And Management, 121: 93–104 (2016).

70. Kayabasi, E., Alperen, M. A., and Kurt, H., "The effects of component dimensions on heat transfer and pressure loss in shell and tube heat exchangers", International Journal Of Green Energy, 16 (2): (2019).

71. Tzivanidis, C., Bellos, E., and Antonopoulos, K. A., "Energetic and financial investigation of a stand-alone solar-thermal Organic Rankine Cycle power plant", Energy Conversion And Management, 126: 421–433 (2016).

72. Akroot, A. and Nadeesh, A., "Performance Analysis of Hybrid Solid Oxide Fuel Cell-Gas Turbine Power System", (2021).

73. Akroot, A., "Effect of Operating Temperatures on the Performance of a SOFCGT Hybrid System", International Journal Of Trend In Scientific Research And Development, Volume-3 (Issue-3): 1512–1515 (2019).

74. Kaya, D., Kayabasi, E., Kilinc, E., Eyidogan, M., Selimli, S., and Ozkaymak, M., "Energy and Exergy Efficiencies in Industrial Pumps", International Journal Of Renewable Energy Resources, 3: 27–42 (2013).

75. Akroot, A. and Namli, L., "Performance assessment of an electrolyte-supported and anode-supported planar solid oxide fuel cells hybrid system", J Ther Eng, 7 (7): 1921–1935 (2021).

76. Nami, H., Mahmoudi, S. M. S., and Nemati, A., "Exergy, economic and environmental impact assessment and optimization of a novel cogeneration system including a gas turbine, a supercritical CO2 and an organic Rankine cycle (GT-HRSG/SCO2)", Applied Thermal Engineering, 110: 1315–1330 (2017).

77. Elmorsy, L., Morosuk, T., and Tsatsaronis, G., "Exergy-based analysis and optimization of an integrated solar combined-cycle power plant", Entropy, 22 (6): 1–20 (2020).

78. Sanaye, S. and Yazdani, M., "Energy, exergy, economic and environmental analysis of a running integrated anaerobic digester-combined heat and power system in a municipal wastewater treatment plant", Energy Reports, 8: 9724–9741 (2022).

79. Soltani, S., Mahmoudi, S. M. S., Yari, M., Morosuk, T., Rosen, M. A., and Zare, V., "A comparative exergoeconomic analysis of two biomass and co-firing combined power plants", Energy Conversion And Management, 76: 83–91 (2013).

80. A Bejan, G Tsatsaronis, M. M., "Thermal Design and Optimization", Energy, 433–434 (1996).

81. Aali, A., Pourmahmoud, N., and Zare, V., "Exergoeconomic analysis and multi-objective optimization of a novel combined flash-binary cycle for Sabalan

geothermal power plant in Iran", Energy Conversion And Management, 143: 377–390 (2017).

82. Wu, C., Wang, S. sen, Feng, X. jia, and Li, J., "Energy, exergy and exergoeconomic analyses of a combined supercritical CO2 recompression Brayton/absorption refrigeration cycle", Energy Conversion And Management, 148: 360–377 (2017).

83. Sahoo, P. K., "Exergoeconomic analysis and optimization of a cogeneration system using evolutionary programming", Applied Thermal Engineering, 28 (13): 1580–1588 (2008).

84. El-Emam, R. S. and Dincer, I., "Exergy and exergoeconomic analyses and optimization of geothermal organic Rankine cycle", Applied Thermal Engineering, 59 (1–2): 435–444 (2013).

85. Pashaei-Didani, H., Nojavan, S., Nourollahi, R., and Zare, K., "Optimal economic-emission performance of fuel cell/CHP/storage based microgrid", International Journal Of Hydrogen Energy, 44 (13): 6896–6908 (2019).

86. Mohammadkhani, F., Shokati, N., Mahmoudi, S. M. S., Yari, M., and Rosen, M. A., "Exergoeconomic assessment and parametric study of a Gas Turbine-Modular Helium Reactor combined with two Organic Rankine Cycles", Energy, 65: 533–543 (2014).

87. Lazzaretto, A. and Tsatsaronis, G., "SPECO: A systematic and general methodology for calculating efficiencies and costs in thermal systems", Energy, 31 (8–9): 1257–1289 (2006).

88. Nourpour, M. and Khoshgoftar Manesh, M. H., "Evaluation of novel integrated combined cycle based on gas turbine-SOFC-geothermal-steam and organic Rankine cycles for gas turbo compressor station", Energy Conversion And Management, 252 (August 2021): 115050 (2022).

89. Elsafi, A. M., "Exergy and exergoeconomic analysis of sustainable direct steam generation solar power plants", Energy Conversion And Management, 103: 338–347 (2015).

90. Wang, Z. Q., Zhou, N. J., Guo, J., and Wang, X. Y., "Fluid selection and parametric optimization of organic Rankine cycle using low temperature waste heat", Energy, 40 (1): 107–115 (2012).

91. Nami, H., Mahmoudi, S. M. S., and Nemati, A., "Exergy, economic and environmental impact assessment and optimization of a novel cogeneration system including a gas turbine, a supercritical CO2 and an organic Rankine cycle (GT-HRSG/SCO2)", Applied Thermal Engineering, 110: 1315–1330 (2017).

92. Behzadi, A., Gholamian, E., Houshfar, E., and Habibollahzade, A., "Multi-objective optimization and exergoeconomic analysis of waste heat recovery from Tehran's waste-to-energy plant integrated with an ORC unit", Energy, 160: 1055–1068 (2018).

93. Wang, S., Liu, C., Li, J., Sun, Z., Chen, X., and Wang, X., "Exergoeconomic analysis of a novel trigeneration system containing supercritical CO2 Brayton cycle, organic Rankine cycle and absorption refrigeration cycle for gas turbine waste heat recovery", Energy Conversion And Management, 221 (May): 113064 (2020).

94. Cavalcanti, E. J. C., .

95. Köse, Ö., Koç, Y., and Yağlı, H., "Energy, exergy, economy and environmental (4E) analysis and optimization of single, dual and triple configurations of the power systems: Rankine Cycle/Kalina Cycle, driven by a gas turbine", Energy Conversion And Management, 227: 113604 (2021).

96. Li, H., Tao, Y., Zhang, Y., and Fu, H., "Two-objective optimization of a hybrid solar-geothermal system with thermal energy storage for power, hydrogen and freshwater production based on transcritical CO2 cycle", Renewable Energy, 183: 51–66 (2022).

97. Deymi-Dashtebayaz, M., Baranov, I. V., Nikitin, A., Davoodi, V., Sulin, A., Norani, M., and Nikitina, V., "An investigation of a hybrid wind-solar integrated energy system with heat and power energy storage system in a near-zero energy building-A dynamic study", Energy Conversion And Management, 269 (May): 116085 (2022).

CURRICULUM VITAE

Abdulrahman AL-TAMIMI is a mechanical engineer who graduated from the faculty of Engineering, University of Karabük - TURKEY. He received his bachelor's degree in 2020. He is currently studying for his master's degree at Karabük University in the field of Mechanical Engineering.